

Effective Theory for Electroweak Doublet Dark Matter

A. DEDES^{1*}, D. KARAMITROS^{1†} AND V. C. SPANOS^{2‡}

¹*Department of Physics, Division of Theoretical Physics,
University of Ioannina, GR 45110, Greece*

²*Section of Nuclear & Particle Physics, Department of Physics,
National and Kapodistrian University of Athens, GR-15784 Athens, Greece*

August 24, 2021

Abstract

We perform a detailed study of an effective field theory which includes the Standard Model particle content extended by a pair of Weyl fermionic $SU(2)$ -doublets with opposite hypercharges. A discrete symmetry guarantees that a linear combination of the doublet components is stable and can act as a candidate particle for Dark Matter. The dark sector fermions interact with the Higgs and gauge bosons through renormalizable $d = 4$ operators, and non-renormalizable $d = 5$ operators that appear after integrating out extra degrees of freedom above the TeV scale. We study collider, cosmological and astrophysical probes for this effective theory of Dark Matter. We find that a WIMP with a mass nearby to the electroweak scale, and thus observable at LHC, is consistent with collider and astrophysical data only when fairly large magnetic dipole moment transition operators with the gauge bosons exist, together with moderate Yukawa interactions.

1 Introduction and Motivation

There is convincing evidence for the existence of Dark Matter (DM) from observation of gravitational effects at astrophysical and cosmological scales but not yet confirmed at Earth's colliders, where interactions between the hypothetical Weakly Interacting DM particle (WIMP) is probed through its interactions with the Standard Model particles (for recent reviews see [1–4]). Out of all energy density in the universe, approximately 25% seems to consist of DM, probably in the form of WIMPs, with its relic density today with respect to the critical density, to be precisely known by the Planck collaboration [5, 6]:

$$\Omega h^2 = 0.1198 \pm 0.0026 . \quad (1.1)$$

Out of many WIMP candidates one of the most studied is the lightest higgsino particle [7, 8], a fermion which is a linear combination of the neutral components of the $SU(2)_L$ -bi-doublet

*email: adedes@cc.uoi.gr

†email: dkaramit@cc.uoi.gr

‡email: vspanos@phys.uoa.gr

superpartners of the Minimal Supersymmetric Standard Model (MSSM) scalar Higgs doublets. A higgsino WIMP fulfilling the constraint of eq. (1.1), which concurrently escapes the direct DM search bounds, must be heavier than the TeV scale, and therefore difficult to be reached at the Large Hadron Collider (LHC).

In this article, we shall consider a “higgsino like” DM sector of the Standard Model (SM) gauge structure, with mass *as close to the electroweak scale as possible*, supplied also by related effective operators of dimension less than or equal to five. Since $SU(2)_L$ fermionic doublets are not singlets under the SM gauge group, there are important interactions already at the renormalizable level, providing annihilation processes of WIMP to SM particles or interactions between the WIMP and the nucleons. Other, what we call “Earth” detectable effects, include contributions to the Electroweak (EW) parameters, to the Higgs boson decay into diphotons, and to other LHC processes, like mono-jets, mono- Z , etc. [9].

Apart from MSSM and its variants, there are many simple models for DM that contain bi-doublets,¹ in their low energy spectrum. For instance, there are models with $SU(2)_L$ doublets+singlet(s) [10–17] or doublets+triplet [18,19]. For EW scale DM at work in most of these models, the need of low energy cut-off, of the order of 1 TeV, is sometimes unavoidable.² In addition, recent attempts to investigate low energy DM-models arising from Grand Unified Theories (e.g., from an $SO(10)$ GUT), seem to incorporate bi-doublets, often in association with other particles, in their low energy particle content [21–23]. This low energy content, may also be part of a non-GUT extension of the Standard Model, as for instance a subgroup of $SO(10)$, such as the left-right symmetric model [24]. There are also Effective Field Theory (EFT) approaches with the $SM+\chi$, or simply SM_χ , where χ is the SM-singlet, up to dimension six effective operators [25,26]. One should remark however, that a light singlet fermionic dark matter is not favoured by $SO(10)$ –GUT constructions consistent with a unification and intermediate symmetry breaking scale at the TeV scale [22,27].

Motivated by all the above we would like to study the phenomenology of a SM with $SU(2)_L$ -bi-doublets with electroweak mass. In terms of physical masses, this model contains a charged Dirac fermion and two Majorana (or Pseudo-Dirac) neutral fermions with their masses splitted with mass differences in the vicinity of tens of GeV due to the presence of $d = 5$ non-renormalizable operators. We study the implications of all the related to dark matter $d = 5$ operators for the relic abundance, for direct as well as indirect searches. A general study of Majorana fermionic dark matter based on SM-extensions of the bi-doublets has been discussed in ref. [28]. Our EFT can be viewed as a decoupling limit of all extra fermion states but not those arising from the $SU(2)_L$ bi-doublet system.

The EFT at hand, generalizes the phenomenology of Standard Models with additional $SU(2)_L$ multiplets, sometimes called Minimal Dark Matter models [29–31]. The most basic of these models is just a Dirac mass term, *c.f.* eq. (2.1), for the bi-doublet fermion multiplet. However, without the imposition of a symmetry the WIMP will not be stable (although higher spin $SU(2)$ -reps will be “accidentally” stable). We discuss in the next section available symmetries that not only protect the WIMP for decaying, like a Z_2 or lepton number, but also forbid potentially dangerous couplings to the Z boson like charge conjugation or custodial

¹By the name “bi-doublets” we mean two Weyl fermion $SU(2)_L$ -doublets with opposite hypercharge.

²It has been shown in ref. [18] that for EW scale DM particle mass one needs relatively large Yukawa couplings between the extra vector-like fermions and the Higgs boson. These lead in turn to vacuum instabilities of the Higgs potential [20], that arise already at the TeV scale, depending on the largeness of the Yukawa couplings and the particle content of the model.

symmetry.

A similar to our EFT, has been studied in ref. [32] for higgsino DM scenario in high scale supersymmetry breaking, using a mass splitting of $\mathcal{O}(\lesssim 1 \text{ GeV})$ originated through $d = 5$ Yukawa interactions and radiative corrections. For higgsino mass parameter $\lesssim \mathcal{O}(1) \text{ TeV}$, the parameter space is constrained from direct detection and Electric Dipole Moment searches. The EFT employed here is complementary to ref. [32]. We assume that the cut-off scale is of order $\Lambda = \mathcal{O}(1 \text{ TeV})$ and for this reason, we introduce a complete set of $d = 5$ operators, *i.e.*, Yukawa and dipole transition operators. We later use all these operators to calculate different observables and constrain the parameter space accordingly. Furthermore, the Yukawa couplings are not restricted by supersymmetry. This, in turn, allows us to focus on larger mass differences and therefore different phenomenology.

As we show in this article, a viable WIMP with mass nearby the electroweak scale acquires fairly large non-zero magnetic dipole moments. Magnetic dipole interacting DM has already been studied in refs. [33–35], a scenario called Magnetic Inelastic Dark Matter (MiDM). In MiDM, the WIMP (χ) is supplemented by a “excited WIMP state”, (χ^*), with $m_{\chi^*} - m_{\chi} = \mathcal{O}(100) \text{ KeV}$. A consequence of this, is a large nucleus-WIMP cross-section, comparable to experimental limits for inelastic nucleus-WIMP scattering. Moreover, in ref. [35], a connection between direct detection and Gamma-ray line signals pointed out, for such small mass splitting. Our work is more general than this scenario, simply because the fermions we introduce are doublets under the $SU(2)_L$. Apart from this, we focus on relatively large mass difference, of order $\mathcal{O}(1 - 10) \text{ GeV}$, between the two neutral fermion states. These facts lead to qualitatively different phenomenology. In particular, the direct detection scattering, in our case, is elastic. Also, due to a symmetry the lightest fermion does not interact directly with Z -boson and the dominant annihilation channels in the early universe are different. Although the EFT studied here is more general from the one suggested previously in the literature, the dipole moments that are responsible for the observed DM relic abundance, provide also enough monochromatic photon flux from the center of our galaxy, to bound considerably (but not to exclude) the parameter space of the model. It is therefore understood that our model could provide an explanation for a possible signal in the near future.

The outline of the article is the following: in section 2 we describe the effective theory and associated possible accidental symmetries and in Appendix A we list the effective $d = 5$ and $d = 6$ operators, that may be present in this extension of the SM. In section 3 we describe the interactions and the mass spectrum. Consequently, in section 4 various collider and direct DM detection constraints are analysed. In addition, in section 5 the DM relic density is calculated, and we study the corresponding cosmological constraints. Moreover, we discuss the phenomenology of possible indirect signals for DM searches, from gamma-rays, and briefly, from neutrino fluxes. In section 6 we study possible signals of this model at LHC at 8 and 13 TeV. Finally, in section 7 we summarise our findings.

2 Symmetries and the effective theory

In the SM particle content we add a fermionic bi-doublet, that is a pair of Weyl fermion $SU(2)$ -doublets with opposite hypercharges, \mathbf{D}_1 , that transform under $(SU(3), SU(2)_L)_Y$ like $(\mathbf{1}^c, \mathbf{2})_{-1}$ and \mathbf{D}_2 , that transform as $(\mathbf{1}^c, \mathbf{2})_{+1}$. The doublet \mathbf{D}_2 has exactly the same gauge quantum numbers as the SM Higgs field \mathbf{H} , while \mathbf{D}_1 carries the quantum numbers of the SM lepton doublet but not necessarily sharing lepton number. Then the model under

study includes gauge invariant kinetic terms like³ $D^{\dagger x a} \bar{\sigma}^{\mu} \mathcal{D}_{\mu} D_{x a}$, with $(x = 1, 2)$ the number of doublets and $(a = 1, 2)$ their $SU(2)_L$ -quantum numbers. These fields have renormalizable couplings with the SM electroweak gauge bosons through \mathcal{D}_{μ} , the covariant derivative for the SM gauge group $SU(2)_L \times U(1)_Y$.

2.1 Custodial symmetry

In addition to gauge invariant kinetic term, an invariant Dirac-type mass term for the bi-doublets is

$$\mathcal{L}_{\text{DM}} \supset -M_D \epsilon^{ab} D_{1a} D_{2b} + \text{H.c.} = -M_D \det \mathcal{D} + \text{H.c.}, \quad (2.1)$$

where ϵ^{ab} is the antisymmetric tensor, with $\epsilon^{12} = -\epsilon^{21} = 1$ and, for later notational use, we define $D_{1a} \equiv (D_1^0, D_1^-)^T$, $D_{2a} \equiv (D_2^+, D_2^0)^T$. In order to make things clearer below, in the second equality of eq. (2.1) we used the definition of the determinant to write the matrix

$$\mathcal{D}_{xa} = (D_{1a} \quad D_{2a}) = \begin{pmatrix} D_1^0 & D_2^+ \\ D_1^- & D_2^0 \end{pmatrix}. \quad (2.2)$$

Written in this form it is now transparent that \mathcal{D} is invariant not only under the $SU(2)_L$ but also under another $SU(2)$, say $SU(2)_R$. The transformation rule under $SU(2)_L \times SU(2)_R$ with corresponding unitary matrices U_L and U_R is

$$\mathcal{D} \rightarrow U_L \mathcal{D} U_R, \quad (2.3)$$

where U_L acts on the rows and U_R acts on the columns of \mathcal{D} , respectively. On the other hand, it is well known [37] that, the SM Higgs sector is also invariant under a global $SU(2)_R$ symmetry. In this case we can write the Higgs field in **(2, 2)** form of $SU(2)_L \times SU(2)_R$ as

$$\mathcal{H}_{ax} = (H_a^* \quad H_a) = \begin{pmatrix} -\Phi^{0*} & \Phi^+ \\ \Phi^- & \Phi^0 \end{pmatrix}. \quad (2.4)$$

Similarly, the Higgs field is invariant under $SU(2)_L \times SU(2)_R$ with a transformation law $\mathcal{H} \rightarrow U_L \mathcal{H} U_R$. Obviously, we can now write down a $SU(2)_L \times SU(2)_R$ non-renormalizable $d = 5$ Yukawa operator as

$$\mathcal{L} \supset \frac{y}{\Lambda} [\text{Tr}(\mathcal{H}^{\dagger} \mathcal{D})]^2 + \text{H.c.} \quad (2.5)$$

where Λ is the scale of masses that are being integrated out. EW symmetry breaking breaks $SU(2)_L \times SU(2)_R$ down to its diagonal subgroup, $SU(2)_{L+R}$. The latter symmetry is the well known *custodial* symmetry [37]. Most pronouncedly it is broken by the difference in magnitude between the top and bottom Yukawa couplings and by the $U(1)_Y$ gauge symmetry but, importantly, keeps radiative EW corrections under control. One of our study benchmarks below arises from eq. (2.5).

2.2 Charge conjugation symmetry

The new \mathbf{D}_1 - and \mathbf{D}_2 -fermion fields form a pseudo-real representation of $SU(2)$. In order to make the presentation transparent, we redefine the Weyl fields as

$$\xi^b = \epsilon^{ab} D_{1a}, \quad \eta_b = D_{2b}, \quad (2.6)$$

³Throughout this paper, we adopt the convenient two-component Weyl spinor notation of ref. [36].

where we can easily arrive at a Dirac fermion field Lagrangian written in terms of the two, two-component Weyl spinor fields, ξ and η , as

$$\mathcal{L}_{\text{DM}} = i\xi_a^\dagger \bar{\sigma}^\mu \mathcal{D}_\mu \xi^a + i\eta^{\dagger a} \bar{\sigma}^\mu \mathcal{D}_\mu \eta_a - M_D (\eta_a \xi^a + \eta^{a\dagger} \xi_a^\dagger). \quad (2.7)$$

The bi-doublets-mass term, M_D , can be taken real and positive. In eq. (2.7), we have suppressed all spinor indices, but have left the gauge group indices intact to show our covariant notation (to be used below). Now, it is well known that the Lagrangian (2.7), beyond $SU(2)_L$ symmetry, accommodates a $O(2)$ -symmetry which, apart from making the usual phase invariance transformation $SO(2) \sim U(1)$ group $\xi \rightarrow e^{-i\theta}\xi$ and $\eta \rightarrow e^{i\theta}\eta$, it contains a discrete symmetry under which

$$C^{-1} \eta_a C = \xi^a. \quad (2.8)$$

This discrete symmetry is a *charge conjugation symmetry (c.c.)*, associated to the charge conjugation operator C with $C^2 = (C^{-1})^2 = I$. This symmetry simply exchanges the two Weyl fields $\xi \leftrightarrow \eta$ or to a “free” notation, $D_1 \leftrightarrow D_2$. There is a similar symmetry in the Higgs sector, where another explicit bi-doublet mass term exists, that of the Higgs field. Then the corresponding charge conjugation symmetry for the Higgs field, which leaves invariant the kinetic terms as well as the Higgs potential in the Standard Model, reads accordingly as,

$$C^{-1} H_a C = H^{\dagger a}, \quad (2.9)$$

where H_a is the SM Higgs doublet, $H_a \equiv (\Phi^+, \Phi^0)^T$. What basically c.c. symmetry does, is to exchange the columns of matrices \mathcal{D} and \mathcal{H} in eqs. (2.2) and (2.4), respectively. For the Higgs field, charge conjugation becomes somewhat trivial for the following reason. In order to read physical masses we have to expand the Lagrangian in terms of fields that vanish at the minimum. There are many $SU(2)_L \times U(1)_Y$ equivalent Higgs representations, but the most known is the so-called Kibble parametrization [38],

$$\mathbf{H} = \mathbf{U} \mathbf{H}_0 = \mathbf{U} \begin{pmatrix} 0 \\ v + \frac{h}{\sqrt{2}} \end{pmatrix}, \quad (2.10)$$

where \mathbf{U} is any 2×2 unitary matrix describing a unitary gauge transformation, v is the vacuum expectation value (vev) [*c.f.* eq. (2.18)], and h is the *real*-valued Higgs field. The matrix \mathbf{U} is absorbed in gauge boson, lepton, quark field redefinitions, *and, in particular* model at hand, in the dark sector fields ξ and η (or D_1 and D_2). Therefore, c.c. symmetry, (2.9), has no effect on \mathbf{H}_0 . On the other hand, the discrete c.c. symmetry in (2.8), acts in a non-trivial way in the dark sector of the model after EW symmetry breaking. We will *assume* that this is a symmetry of the Lagrangian and examine implications from this hypothesis.

2.3 The discrete Z_2 -symmetry

Unfortunately, the c.c. or the custodial symmetries alone can not account for the stability of DM lightest particle and an extra discrete Z_2 -symmetry that distinguishes SM-particles from DM-particles is needed. To “throw away” dangerous $d = 4$ operators that are responsible for WIMP decay, like $D_1 H^\dagger \bar{e}$ or higher [see Appendix A for assignments and in particular eq. (A.4)], it could be enough to impose a lepton number symmetry for example. It is safer however, to impose an external Z_2 -discrete symmetry under which the SM fermions are odd while the dark matter fermions and the Higgs boson are even eigenstates. Such a discrete

symmetry, or equivalently, its variant known from MSSM as R-parity, is preserved in $SO(10)$ with the Higgs field in a **126** representation [39] and are common in Grand Unified Theories (GUTs) with low mass dark matter particles [21–23, 40]. We shall therefore assume such a Z_2 -symmetry in what follows.

2.4 Symmetric limits used in the analysis

Our model, is based on an effective theory described by the following Lagrangian:

$$\mathcal{L} = \mathcal{L}_{\text{SM}} + \mathcal{L}_{\text{DM}} + \mathcal{L}_{\text{SM+DM}}^{d=5}. \quad (2.11)$$

\mathcal{L}_{SM} is the SM renormalizable Lagrangian, \mathcal{L}_{DM} is the DM sector renormalizable Lagrangian given by eq. (2.7) and $\mathcal{L}_{\text{SM+DM}}^{d=5}$ is the Lagrangian that contains the dimension-5 operators relevant to DM interactions. We assume that higher dimensional operators ($d \geq 6$) are suppressed and throughout this article we are focusing on up-to $d = 5$ effective operators. For the sake of completeness, however, in Appendix A we construct all relevant operators for both dimensionalities $d = 5$ and $d = 6$.

We show below that by using the the c.c. symmetry of eq. (2.8), or the custodial symmetry or just the $U(1)$ phase symmetry we can arrive at four distinct choices in the parameter space. Moreover, this is very convenient for the phenomenological study that follows. First, $\mathcal{L}_{\text{SM+DM}}^{d=5}$ contains effective operators that after spontaneous EW symmetry breaking split the masses of the neutral particles from their original common mass M_D . The most general, linearly independent set of operators, is

$$\begin{aligned} -\mathcal{L}_{\text{SM+DM}}^{d=5} \supset & \quad \frac{y_1}{2\Lambda} (H_a \xi^a) (H_b \xi^b) + \frac{y_2}{2\Lambda} (H^{\dagger a} \eta_a) (H^{\dagger b} \eta_b) - \frac{y_{12}}{\Lambda} (H_a \xi^a) (H^{\dagger b} \eta_b) \\ & + \frac{\xi_{12}}{\Lambda} (\xi^a \eta_a) (H^{\dagger b} H_b) + \text{H.c.} \end{aligned} \quad (2.12)$$

where Λ is the cutoff of the effective, SM+bi-doublet, theory.⁴ If the c.c. symmetry (2.8) is imposed the last two terms of eq. (2.12) are unaffected, but the first two terms must be the same. This means that under c.c. symmetry the relation

$$y_1 = y_2 \equiv y, \quad (2.13)$$

holds. We always follow this symmetry condition in the analytical expressions as well in the numerical results throughout this article. Even more, one can write the independent c.c. symmetry invariant $d = 5$ operators

$$y (H_a \xi^a - H^{\dagger a} \eta_a)^2 \quad \text{or} \quad y (H_a \xi^a + H^{\dagger a} \eta_a)^2, \quad (2.14)$$

in addition to the operators multiplying y_{12} and ξ_{12} in eq. (2.12). Based on symmetries discussed above, there are additional restrictions on Yukawa couplings

$$(1) y = y_{12}, \quad (2) y = -y_{12}, \quad (3) y_{12} = 0, \quad (4) y = y_{12} = 0, \quad \forall y, \quad \forall \xi_{12}. \quad (2.15)$$

Cases (1) and (2) above, may correspond to the $SU(2)_L \times SU(2)_R$ symmetry limit of eq. (2.5). Case (3) is not really supported by any symmetry consideration, in fact it violates the custodial

⁴In eq. (A.1) we give examples of what sort of heavy particle mass the Λ might be.

symmetry, and is only adopted here for covering the mass spectrum phenomenology (*c.f.* Fig. 1). In choosing the benchmark for case (4) we are motivated by the following: in a full gauge invariant theory, y_{12} and ξ_{12} may have certain relations with y . For example, in the fermionic doublet-triplet DM model of ref. [18] one finds $\xi_{12} = -2y = 2y_{12}$ after decoupling the heavy triplet in the custodial limit. If the continuous $U(1)$ -phase symmetry is employed (or if the two $SU(2)_R$ symmetries for \mathcal{D} and \mathcal{H} are different) then $y = 0$ for all y_{12} and ξ_{12} . In this case there are two, mass degenerate, Dirac fermions in the spectrum: one neutral and one charged. This completes our study benchmark points which are mostly based upon the underlying global symmetries of the model rather on a random choice of the model parameters.

There are also $d = 5$ magnetic and electric dipole operators related to the dark sector particles. A detailed form of these operators is given in Appendix A. In this article we shall focus on the magnetic dipole operators

$$-\mathcal{L}_{\text{SM+DM}}^{d=5} \supset \frac{d_\gamma}{\Lambda} \xi^a \sigma^{\mu\nu} \eta_a B_{\mu\nu} + \frac{d_W}{\Lambda} \xi^b \sigma^{\mu\nu} (\tau^A)_b^c \eta_c W_{\mu\nu}^A + \text{H.c.}, \quad (2.16)$$

where $B_{\mu\nu}$ and $W_{\mu\nu}^A$ are the $U(1)_Y$ and $SU(2)_L$ field strength tensors respectively and τ^A the Pauli matrices with $A = 1, 2, 3$ and $\sigma^{\mu\nu} \equiv \frac{i}{4}(\sigma^\mu \bar{\sigma}^\nu - \sigma^\nu \bar{\sigma}^\mu)$. These operators are invariant under (2.8) since $C^{-1} \xi \sigma^{\mu\nu} \eta C = \eta \sigma^{\mu\nu} \xi = -\xi \sigma^{\mu\nu} \eta$, $C^{-1} W_{\mu\nu}^A C = (-1)^{2-A} W_{\mu\nu}^A$ (no sum in A) and $C^{-1} B_{\mu\nu} C = -B_{\mu\nu}$. We shall see below that both moments d_γ and d_W , play an important role in achieving the correct relic density.

As promised earlier in this section, the new, beyond the SM parameters needed to describe the dark sector are the following six:

$$M_D, \quad \Lambda, \quad y, \quad \xi_{12}, \quad d_\gamma, \quad d_W. \quad (2.17)$$

Throughout, we assume them all to be real. More importantly, we *assume* that the mass M_D is around or below the EW-scale, that is of the order of $\mathcal{O}(100)$ GeV. The mass scale Λ for extra scalars and fermions, are far above the EW scale, possibly at the TeV-scale. As a result, we assume that this EFT contains three (but two distinct) mass scales,

$$M_D \simeq v \simeq 174 \text{ GeV}, \quad \Lambda \simeq \mathcal{O}(1) \text{ TeV}. \quad (2.18)$$

3 Phenomenology

3.1 Mass Spectrum

After electroweak symmetry breaking and the shift of the neutral component of the Higgs field $H_0 = (0, v + h/\sqrt{2})^T$, in eqs. (2.7) and (2.12), we obtain

$$\mathcal{L}_{(\text{mass})}^{\text{DM}} = -m_{\chi^\pm} \chi^- \chi^+ - \frac{1}{2} \sum_{i=1}^2 m_{\chi_i^0} \chi_i^0 \chi_i^0 + \text{H.c.}, \quad (3.1)$$

where, under the c.c. symmetry restrictions (2.13), the physical fields are two neutral Majorana fermions (χ_1^0, χ_2^0) and one pair of Dirac charged fermions (χ^\pm)

$$\chi_1^0 = \frac{1}{\sqrt{2}} (D_1^0 + D_2^0), \quad \chi_2^0 = -\frac{i}{\sqrt{2}} (D_1^0 - D_2^0), \quad (3.2a)$$

$$\chi^+ = i D_2^+, \quad \chi^- = i D_1^-, \quad (3.2b)$$

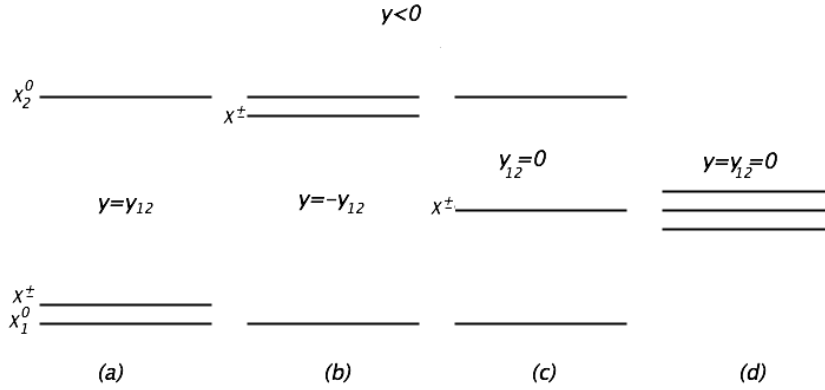


Figure 1: Mass hierarchies of the dark fermions χ_1^0 , χ^\pm and χ_2^0 (bottom to top) for $y < 0$, following the c.c. symmetry of eq. (2.15) for the cases (a) $y = y_{12}$, (b) $y = -y_{12}$, (c) $y_{12} = 0$ and (d) $y = y_{12} = 0$. The mass spectrum for $y > 0$ is obtained from this figure by exchanging $\chi_1^0 \leftrightarrow \chi_2^0$.

with masses,

$$m_{\chi^\pm} = M_D + \xi_{12} \omega, \quad (3.3a)$$

$$m_{\chi_1^0} = m_{\chi^\pm} + \omega (y - y_{12}), \quad \omega \equiv \frac{v^2}{\Lambda}, \quad (3.3b)$$

$$m_{\chi_2^0} = m_{\chi^\pm} - \omega (y + y_{12}). \quad (3.3c)$$

Without loss of generality, our natural choice for field redefinitions is such that $M_D > 0$. Under the c.c. symmetry the state χ_1^0 is even, while the states χ_2^0, χ^\pm are odd, *i.e.*,

$$C^{-1} \chi_1^0 C = +\chi_1^0, \quad C^{-1} \chi_2^0 C = -\chi_2^0, \quad (3.4)$$

$$C^{-1} \chi^+ C = -\chi^-, \quad C^{-1} \chi^- C = -\chi^+. \quad (3.5)$$

However, in general and far from custodial symmetry limits, only χ^+ and χ^- are particle-antiparticle states with common mass, m_{χ^\pm} .

In what follows, we sort the masses so that the lightest particle is χ_1^0 . Also, we assume $M_D + \xi_{12} \omega > 0$, for otherwise the contribution from $d = 5$ operators to the masses, *i.e.*, the term $\xi_{12} \omega$ would be unnaturally large, in order to satisfy the LEP bound [41–43] $m_{\chi^\pm} \gtrsim 100$ GeV. There are two equivalent set of mass spectra: one with $y \leq 0$ where $m_{\chi_1^0} \leq m_{\chi_2^0}$ and the other $y \geq 0$ where $m_{\chi_2^0} \leq m_{\chi_1^0}$. In Fig. 1, we show the spectrum for the $y \leq 0$ case. The mass spectrum for $y > 0$ is exactly the same after exchanging $\chi_1^0 \leftrightarrow \chi_2^0$. We note that the mass hierarchies between χ^\pm , χ_1^0 and χ_2^0 displayed in Fig. 1 do not depend on M_D and ξ_{12} , although their central mass values are all shifted uniformly upon their variation. Therefore, following eq. (2.15), we distinguish four mass spectra:

(a) $y = y_{12} < 0$: the lightest neutral DM fermion χ_1^0 is almost degenerate with the charged one χ^\pm (see Fig. 1a) with

$$m_{\chi_1^0} = m_{\chi^\pm}, \quad m_{\chi_2^0} = m_{\chi^\pm} + 2\omega|y|. \quad (3.6)$$

(b) $y = -y_{12} < 0$: the heavy neutral fermion χ_2^0 is degenerate with the charged fermion

χ^\pm (Fig. 1b) with

$$m_{\chi_1^0} = m_{\chi^\pm} - 2\omega|y|, \quad m_{\chi_2^0} = m_{\chi^\pm}. \quad (3.7)$$

(c) $y_{12} = 0, \forall y < 0$: all χ_1^0 and χ_2^0 are split from χ^\pm by an equal amount $\omega|y|$ with (Fig. 1c)

$$m_{\chi_1^0} = m_{\chi^\pm} - \omega|y|, \quad m_{\chi_2^0} = m_{\chi^\pm} + \omega|y|. \quad (3.8)$$

(d) $y_{12} = y = 0$: all four particles and antiparticles are degenerate in mass (Fig. 1d)

$$m_{\chi_1^0} = m_{\chi^\pm} = m_{\chi_2^0}. \quad (3.9)$$

This case describes two Dirac fields: one neutral and one charged. It can be viewed as a limit of case (c) when $y \rightarrow 0$. All these mass relations have been derived at tree level. However, it is known that these mass differences are altered by a finite piece of $\mathcal{O}(100 - 1000 \text{ MeV})$, when radiative corrections are taken into account [44]. Even in the custodial symmetry limit, these corrections should be proportional to the $U(1)_Y$ gauge coupling. They are small compared to $\omega|y|$ contributions to the masses from the $d = 5$ operators when the scale Λ is low, e.g., $\mathcal{O}(1)$ TeV. As a result, the mass hierarchies depicted in Fig. 1 will survive beyond tree level in all cases apart from case (d).

3.2 Dark Matter Particle Interactions

Our notation follows closely that of ref. [18]. We calculate the Higgs interactions with the extra fermions from eq. (2.12). We find,

$$\begin{aligned} \mathcal{L}_{Y(\text{int})}^{\text{DM}} = & -Y^{h\chi^- \chi^+} h \chi^- \chi^+ - \frac{1}{2} Y^{h\chi_i^0 \chi_j^0} h \chi_i^0 \chi_j^0 \\ & - \frac{1}{2} Y^{hh\chi^- \chi^+} h h \chi^- \chi^+ - \frac{1}{4} Y^{hh\chi_i^0 \chi_j^0} h h \chi_i^0 \chi_j^0 + \text{H.c.}, \end{aligned} \quad (3.10)$$

where

$$Y^{h\chi^- \chi^+} = \sqrt{2} \xi_{12} \frac{\omega}{v}, \quad Y^{hh\chi^- \chi^+} = \xi_{12} \frac{\omega}{v^2}, \quad (3.11a)$$

$$Y^{h\chi_1^0 \chi_1^0} = \frac{\sqrt{2}\omega}{v} (\xi_{12} + y - y_{12}), \quad Y^{hh\chi_1^0 \chi_1^0} = \frac{\omega}{v^2} (\xi_{12} + y - y_{12}), \quad (3.11b)$$

$$Y^{h\chi_2^0 \chi_2^0} = \frac{\sqrt{2}\omega}{v} (\xi_{12} - y - y_{12}), \quad Y^{hh\chi_2^0 \chi_2^0} = \frac{\omega}{v^2} (\xi_{12} - y - y_{12}), \quad (3.11c)$$

$$Y^{h\chi_1^0 \chi_2^0} = 0, \quad Y^{hh\chi_1^0 \chi_2^0} = 0. \quad (3.11d)$$

The 4-point $h^2\chi^2$ vertices are proportional to 3-point $h\chi^2$ vertices. Interestingly enough, off-diagonal couplings to h in (3.11d), vanish identically due to the c.c. symmetry of eqs. (3.4) and (3.5), using that $C^{-1}hC = h$.

Since D_1 and D_2 carry $SU(2)_L \times U(1)_Y$ quantum numbers, there are renormalizable interactions involving gauge bosons and the dark fermions, $\chi_{1,2}^0$ and χ^\pm . For instance, the interaction between χ^\pm and the photon reads

$$\mathcal{L}_{\text{KIN}(\text{int})}^{\gamma-\chi^\pm} = -(+e) (\chi^+)^\dagger \bar{\sigma}^\mu \chi^+ A_\mu - (-e) (\chi^-)^\dagger \bar{\sigma}^\mu \chi^- A_\mu, \quad (3.12)$$

where A_μ is the photon field and $(-e)$ the electron electric charge. Similarly, the Z -gauge boson couplings to charged and neutral dark fermions are

$$\mathcal{L}_{\text{KIN(int)}}^{Z-\chi} = \frac{g}{c_W} O'^L (\chi^+)^\dagger \bar{\sigma}^\mu \chi^+ Z_\mu - \frac{g}{c_W} O'^R (\chi^-)^\dagger \bar{\sigma}^\mu \chi^- Z_\mu + \frac{g}{c_W} O''^L (\chi_i^0)^\dagger \bar{\sigma}^\mu \chi_j^0 Z_\mu, \quad (3.13)$$

where

$$O'^L = O'^R = -\frac{1}{2}(1 - 2s_W^2), \quad (3.14a)$$

$$O''^L = \frac{1}{2} (O_{2i}^* O_{2j} - O_{1i}^* O_{1j}), \quad (3.14b)$$

$$O = \frac{1}{\sqrt{2}} \begin{pmatrix} 1 & i \\ 1 & -i \end{pmatrix}, \quad O''^L = -\frac{i}{2} \begin{pmatrix} 0 & 1 \\ -1 & 0 \end{pmatrix}. \quad (3.14c)$$

With s_W (c_W) we denote the $\sin \theta_W$ ($\cos \theta_W$) of the weak mixing angle and with g the $SU(2)_L$ gauge coupling. The coupling $Z \chi_i^0 \chi_j^0$ is non-zero only for $i \neq j$ due to the c.c. symmetry with $C^{-1} Z_\mu C = -Z_\mu$. The O''^L is an antisymmetric matrix due to the Majorana nature of χ_i^0 fermions and the hermiticity of the Lagrangian.

Interactions between χ 's and W -bosons are described by the following terms

$$\begin{aligned} \mathcal{L}_{\text{KIN(int)}}^{W^\pm-\chi^0-\chi^\mp} &= g O_i^L (\chi_i^0)^\dagger \bar{\sigma}^\mu \chi^+ W_\mu^- - g O_i^R (\chi^-)^\dagger \bar{\sigma}^\mu \chi_i^0 W_\mu^- \\ &+ g O_i^{L*} (\chi^+)^\dagger \bar{\sigma}^\mu \chi_i^0 W_\mu^+ - g O_i^{R*} (\chi_i^0)^\dagger \bar{\sigma}^\mu \chi^- W_\mu^+, \end{aligned} \quad (3.15)$$

where the mixing column matrices O^L and O^R are given by

$$O_i^L = \frac{i}{\sqrt{2}} O_{2i}^* = \frac{1}{2} \begin{pmatrix} i \\ -1 \end{pmatrix}, \quad (3.16a)$$

$$O_i^R = \frac{i}{\sqrt{2}} O_{1i} = \frac{1}{2} \begin{pmatrix} i \\ -1 \end{pmatrix}, \quad (3.16b)$$

with the identity $O_i^R = O_i^L$ being again a consequence of the c.c. symmetry. Using the same matrices we can write the three-point dipole interactions of eq. (A.5) in the diagonal basis ⁵

$$\begin{aligned} \mathcal{L}_{\text{dipole}}^{3\text{-point}} &= -\frac{\omega}{v^2} (d_\gamma s_W + d_W c_W) O_{ij}''^L \chi_i^0 \sigma_{\mu\nu} \chi_j^0 F_Z^{\mu\nu} - \frac{\omega}{v^2} (d_\gamma s_W - d_W c_W) \chi^- \sigma_{\mu\nu} \chi^+ F_Z^{\mu\nu} \\ &+ \frac{\omega}{v^2} (d_\gamma c_W - d_W s_W) O_{ij}''^L \chi_i^0 \sigma_{\mu\nu} \chi_j^0 F_\gamma^{\mu\nu} + \frac{\omega}{v^2} (d_\gamma c_W + d_W s_W) \chi^- \sigma_{\mu\nu} \chi^+ F_\gamma^{\mu\nu} \\ &- 2\frac{\omega}{v^2} d_W O_i^{R*} \chi^- \sigma_{\mu\nu} \chi_i^0 F_{W^+}^{\mu\nu} + 2\frac{\omega}{v^2} d_W O_i^L \chi^+ \sigma_{\mu\nu} \chi_i^0 F_{W^-}^{\mu\nu} + \text{H.c.}, \end{aligned} \quad (3.17)$$

where $F_V^{\mu\nu} = \partial^\mu V^\nu - \partial^\nu V^\mu$, $V = Z, A$ and W^\pm . Interestingly enough, EFT dipole $d = 5$ operators, generate photon interactions with the neutral dark particles, with a coupling that vanishes in the limit $d_\gamma c_W \simeq d_W s_W$. There is also an alignment of couplings in eq. (3.17) with the those in eqs. (3.13) and (3.15), that is important for achieving a ‘‘natural’’ cancellation of two different contributions in the cross-section for $\chi_1^0 \chi_1^0 \rightarrow VV$, where V can be Z, W or

⁵We are not concerned here about CP-violating phenomena and we set $e_{\gamma, W} = 0$.

γ . Moreover, the four-point interactions involving dipole operators are

$$\begin{aligned}
\mathcal{L}_{\text{dipole}}^{4\text{-point}} &= -2ig \frac{\omega}{v^2} d_W O_{ij}^{\prime L} \chi_i^0 \sigma_{\mu\nu} \chi_j^0 W^{+\mu} W^{-\nu} + 2ig \frac{\omega}{v^2} d_W \chi^- \sigma_{\mu\nu} \chi^+ W^{+\mu} W^{-\nu} \\
&+ 4ig \frac{\omega}{v^2} d_W c_W O_i^{R*} \chi^- \sigma_{\mu\nu} \chi_i^0 W^{+\mu} Z^\nu + 4ig \frac{\omega}{v^2} d_W c_W O_i^L \chi^+ \sigma_{\mu\nu} \chi_i^0 W^{-\mu} Z^\nu \\
&+ 4ig \frac{\omega}{v^2} d_W s_W O_i^{R*} \chi^- \sigma_{\mu\nu} \chi_i^0 W^{+\mu} A^\nu + 4ig \frac{\omega}{v^2} d_W s_W O_i^L \chi^+ \sigma_{\mu\nu} \chi_i^0 W^{-\mu} A^\nu \\
&+ \text{H.c.}
\end{aligned} \tag{3.18}$$

In section 5, we will see that these EFT dipole interactions are important for making the annihilation and coannihilation cross section of the WIMP dark matter particle χ_1^0 , compatible with the measurement (1.1) for the DM relic density.

4 “Earth” constraints in the Dark Sector

In this section we study constraints imposed on the parameter space, from WIMP(χ_1^0)-nucleon scattering experiments searching directly for DM, from direct and oblique LEP electroweak observables and from the LHC data for the Higgs boson decay to two photons.

4.1 Nucleon-WIMP direct detection experimental bounds

In the limit that the DM particle χ_1^0 is much heavier than nucleon, the spin independent (SI) and spin dependent (SD) cross sections are given by [45]

$$\sigma_{\text{SI}} = 8 \times 10^{-45} \text{ cm}^2 \left(\frac{Y^{h\chi_1^0\chi_1^0}}{0.1} \right)^2, \quad \sigma_{\text{SD}} = 3 \times 10^{-39} \text{ cm}^2 \left(\frac{g^{Z\chi_1^0\chi_1^0}}{0.1} \right)^2. \tag{4.1}$$

From the interactions in eq. (3.13), we see that $g^{Z\chi_1^0\chi_1^0} = 0$ at tree level and therefore $\sigma_{\text{SD}} \approx 0$. For the SI cross-section the current bound from LUX [46, 47] is $\sigma_{\text{SI}} \simeq \{1 - 3.5\} \times 10^{-45} \text{ cm}^2$, for $m_{\text{DM}} \simeq \{100 - 500\} \text{ GeV}$, respectively. This gives

$$|Y^{h\chi_1^0\chi_1^0}| \lesssim \{0.04, 0.06\}, \tag{4.2}$$

which through the r.h.s. of eq. (3.11b) yields a constraint for the combination $\xi_{12} + y - y_{12}$. The one-loop contributions have been calculated in refs. [18, 19]. We have worked out the formula given in the Appendix A of ref. [18], for zero Yukawa couplings and $M_D \gg M_{W,Z}$, and we find

$$\delta Y^{h\chi_1^0\chi_1^0} = \left(\frac{3g}{8\pi} \right)^2 \frac{\sqrt{2}M_Z}{v} \frac{M_D - M_Z}{M_D} \simeq 4 \times 10^{-3}. \tag{4.3}$$

This is an order of magnitude smaller⁶ than the current LUX bound in eq. (4.2). In the limit $M_D \rightarrow \infty$, the model exhibits a non-decoupling behaviour, as expected from the EFT analysis of refs. [29, 49, 50]. On the other hand, for $M_D \rightarrow 0$ the one-loop contribution vanishes.

Based upon eqs. (3.11b) and (4.2) we obtain the inequality

$$|\xi_{12} + y - y_{12}| \leq \frac{1}{\sqrt{2}} \left(\frac{\Lambda}{v} \right) Y^{\text{bound}}(m_{\chi_1^0}), \tag{4.4}$$

⁶It is shown in ref. [48] that for next to leading order corrections in α_s , the SI cross-section is even smaller.

where $Y^{\text{bound}}(m_{\chi_1^0})$ is the bound of eq. (4.2). Eq. (4.4) sets strong bounds on the couplings ξ_{12} and/or y . Relevant to the cases depicted in Fig. 1 we obtain, for $\Lambda = 1$ TeV and $m_{\chi_1^0} \sim 100$ GeV the following constraints:

$$\begin{aligned}
\text{(a, d)} : \quad & -0.16 \lesssim \xi_{12} \lesssim 0.16 , \\
\text{(b)} : \quad & -\frac{16 + 200 y}{100} \lesssim \xi_{12} \lesssim \frac{16 - 200 y}{100} , \\
\text{(c)} : \quad & -\frac{16 + 100 y}{100} \lesssim \xi_{12} \lesssim \frac{16 - 100 y}{100} .
\end{aligned} \tag{4.5}$$

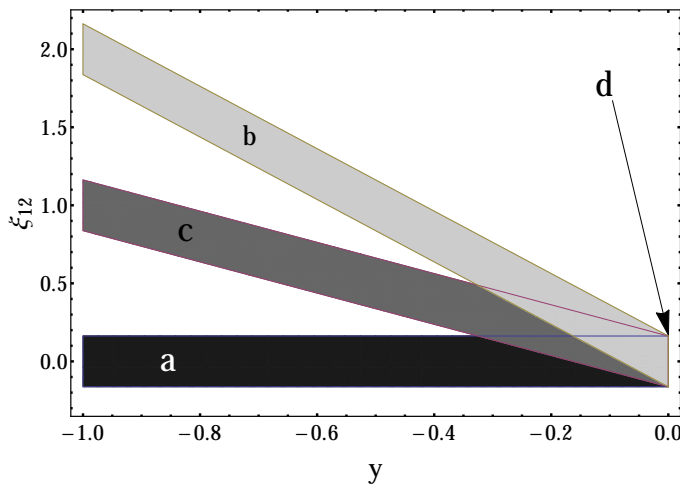


Figure 2: *Yukawa couplings y vs. ξ_{12} compatible with the bound of eq. (4.2) related to the LUX DM detection experiment, for the four cases of the mass spectrum and $\Lambda = 1$ TeV.*

Therefore, for $y \sim -1$, the parameter ξ_{12} is always positive with a small variation band of about 10% w.r.t. the $|y|$ value due to the LUX bound. An example for the case (c) is shown in Fig. 2. For even bigger values of $|y|$, we obtain, ξ_{12} as big as $|y|$ for case (c) or as big as $2|y|$ in case (b). The band of the allowed values for ξ_{12} , e.g., the shaded area in Fig. 2, expands if we increase Λ .

Apparently, from eq. (3.3), if $y = 0$ we get $m_{\chi_1^0} = m_{\chi_2^0}$. In addition, if dipole operators of eq. (3.17) are present, severe bounds on d_γ and d_W can be set based on contribution to WIMP-nucleon cross section from γ, Z -exchange graphs [51–53]. In our case these bounds are avoided because we choose always $m_{\chi_2^0} - m_{\chi_1^0} \gtrsim 2$ GeV [33].

It is worth repeating here, that ξ_{12} is in principle positive everywhere for the cases (b,c), which means that essentially the charged particle χ^\pm is behaving as an extra lepton circulating in the $h \rightarrow \gamma\gamma$ loop decay process. Therefore, we expect that $R_{h \rightarrow \gamma\gamma}$ will be in general smaller than in the SM.

4.2 LEP bounds

Next we examine constrains from LEP, that although have been derived particularly for the MSSM, they can easily be adapted to this model. From Fig. 1 we observe that always, the

next-to-lightest particle is the charged dark fermion χ^\pm with mass $m_{\chi^\pm} = M_D + \xi_{12}\omega$ that, as explained before, is assumed to be positive.

Depending on the mass difference between the lightest neutral particle $m_{\chi_1^0}$ and the charged one m_{χ^\pm} , the bound on m_{χ^\pm} varies within ~ 90 GeV to ~ 100 GeV [41–43]. We will use the most conservative choice

$$m_{\chi^\pm} \gtrsim 100 \text{ GeV} , \quad (4.6)$$

which in terms of ξ_{12} , ω and M_D becomes:

$$\xi_{12} \gtrsim \frac{100 - M_D}{\omega}, \quad \forall y_{12} . \quad (4.7)$$

As we have seen, the bound from direct detection experiments implies a positive value on ξ_{12} for the cases (b,c). Thus, the LEP bound (4.7) is always satisfied if $M_D \gtrsim 100$ GeV. In the case where $M_D \lesssim 100$ GeV one may evade the LEP bound with a large positive ξ_{12} . For example, for $\Lambda = 1$ TeV and $M_D = 50$ GeV, we need, $\xi_{12} \gtrsim 1.7$. Interestingly, this may be compatible with (4.5) only in cases (b) and (c) with $\Lambda = 1$ TeV and certain values of y .

4.3 $h \rightarrow \gamma\gamma$

For the model under study, the ratio $R_{h \rightarrow \gamma\gamma} \equiv \frac{\Gamma(h \rightarrow \gamma\gamma)}{\Gamma(h \rightarrow \gamma\gamma)_{\text{SM}}}$ is given by [18]

$$R_{h \rightarrow \gamma\gamma} = \left| 1 + \frac{1}{A_{\text{SM}}} \frac{\sqrt{2} Y^{h\chi^- \chi^+} v}{m_{\chi^\pm}} A_{1/2}(\tau) \right|^2 , \quad (4.8)$$

where $A_{\text{SM}} \simeq -6.5$ for $m_h = 125$ GeV. This is the SM result dominated by the W -loop, with $\tau \equiv m_h^2/4m_{\chi^\pm}^2$ and $A_{1/2}$ is the well known function given for example in ref. [54]. The ratio R is currently under experimental scrutiny at LHC. The current combined value is $R_{h \rightarrow \gamma\gamma} = 1.15_{-0.25}^{+0.28}$ [55]. Note that the gluon fusion channel $gg \rightarrow h$, involved in the Higgs boson production at LHC, is not affected in the context of this model, since χ_i^0, χ^\pm are uncoloured particles. In principle, there are $d = 6$ operators, such as $H^\dagger H G_{\mu\nu} G^{\mu\nu}$, but we assume that these are quite suppressed in comparison to the SM contribution. An analogous operator exists in the case of $h \rightarrow \gamma\gamma$, just replacing $G^{\mu\nu}$ with the photon field strength tensor, $F^{\mu\nu}$ when integrated out heavy (of order bigger than Λ) particles. These operators arise at loop level and are suppressed by the scale Λ . Therefore, for the process $h \rightarrow \gamma\gamma$, the effect is dominated by the SM charged particles and the new χ^\pm circulating in the triangle diagram.

Below we study the ratio R in two complementary regions for M_D : a) $M_D \lesssim 100$ GeV and b) $M_D \gtrsim 100$ GeV.

4.3.1 $M_D \lesssim 100$ GeV

From eq. (3.11a) we expect that ξ_{12} would be restricted to small values from the loop induced $h \rightarrow \gamma\gamma$ bound, where we should also expect that, for M_D below 100 GeV, the bound from LEP will be important as we explained previously in section 4.2. When $M_D \lesssim 100$ GeV, ξ_{12} should always be positive or zero in order to satisfy the LEP bound (4.7). Then the charged fermion behaves as an extra lepton and lowers the ratio R . This is clear from eqs. (3.11a) and (4.8). In addition, one can easily observe that, since LEP restricts m_{χ^\pm} to be above 100 GeV,

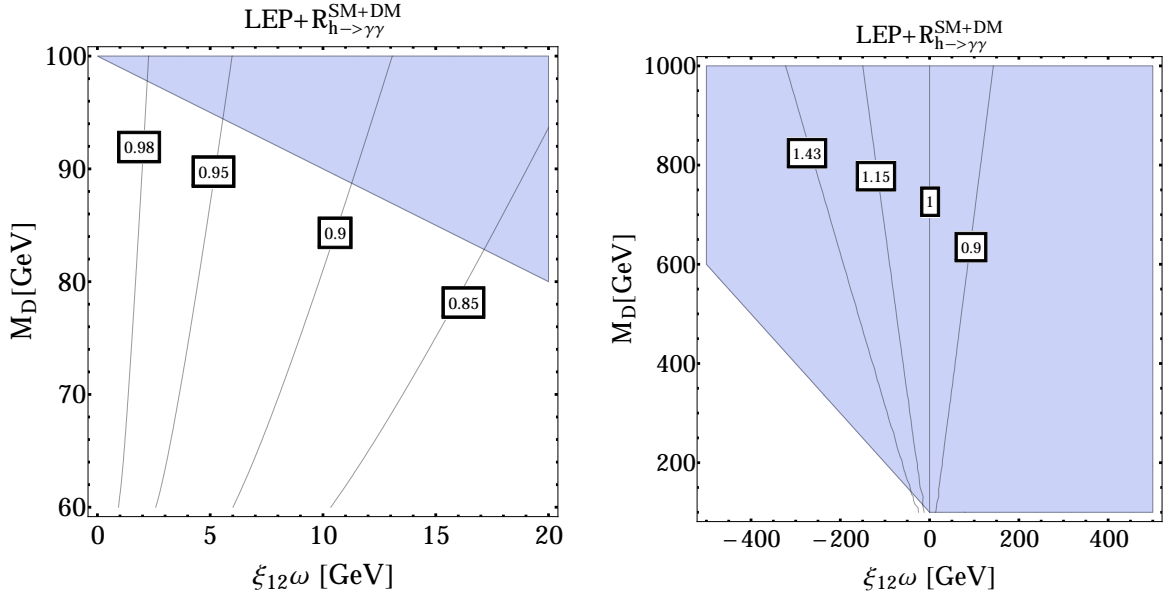


Figure 3: Combination of the constraints from negative LEP “chargino” searches applied to χ^\pm and the ratio $R_{h \rightarrow \gamma\gamma}$ from LHC (Run I), for (a) $M_D \lesssim 100$ GeV and (b) $M_D \gtrsim 100$ GeV. The shaded region is compatible to the LEP χ^\pm bound, while the contours show the values of $R_{h \rightarrow \gamma\gamma}$ from eq. (4.8) on $\xi_{12}\omega - M_D$ plane.

the function $A_{1/2}(\tau = m_h^2/4m_{\chi^\pm})$ lies within the interval $\sim 1.5 - 1.3$. These observations lead us to another improved bound between ξ_{12} , ω and M_D , for the combined constraints from LEP and $R_{h \rightarrow \gamma\gamma}$:

$$100 - M_D \lesssim \xi_{12}\omega \lesssim 0.1 M_D, \quad \forall y_{12}. \quad (4.9)$$

Therefore, if $M_D \lesssim 100$ GeV, we obtain a minimum allowed value for M_D , which is around 90 GeV, as illustrated in Fig. 3(a). As a consequence, the case $M_D \lesssim 100$ GeV is disfavoured.

4.3.2 $M_D \gtrsim 100$ GeV

If $\xi_{12} > 0$, then eq. (4.9) still holds. The only difference from the previous case arises from eq. (4.7), which now allows ξ_{12} to be also negative. Consequently, for $\xi_{12} < 0$, the $R_{h \rightarrow \gamma\gamma}$ can be greater than unity and we obtain

$$\xi_{12}\omega \gtrsim -0.3 M_D, \quad \text{or} \quad \xi_{12}\omega \gtrsim 100 - M_D, \quad \forall y_{12} \text{ and } \xi < 0. \quad (4.10)$$

Therefore, the combined result for $M_D \gtrsim 100$ GeV is:

$$-0.3 M_D \lesssim \xi_{12}\omega \lesssim 0.1 M_D \quad \text{and} \quad \xi_{12}\omega \gtrsim 100 - M_D, \quad \forall y_{12}. \quad (4.11)$$

This inequality is illustrated in Fig. 3(b). We notice that eq. (4.11) results in a very weak bound for $\xi_{12} < 0$ compared to the constraints from direct detection experiments, as can be seen in Fig. 2. Eq. (4.11) may nicely be combined in terms of the physical charged fermion mass m_{χ^\pm} and the “doublet” mass M_D as

$$0.7 M_D \lesssim m_{\chi^\pm} \lesssim 1.1 M_D. \quad (4.12)$$

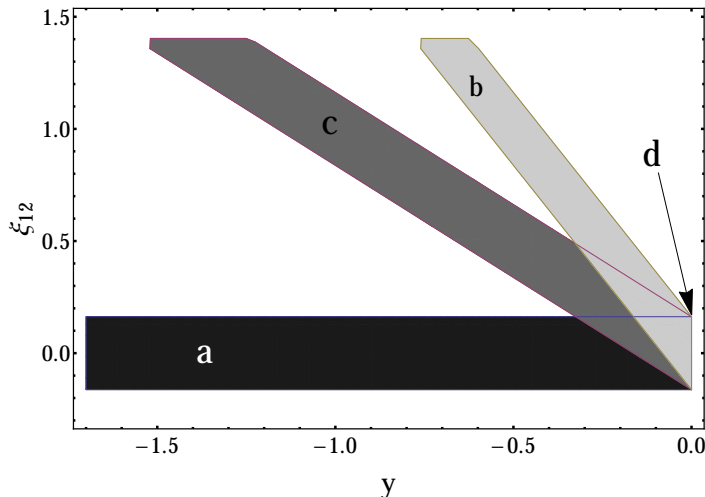


Figure 4: y vs. ξ_{12} regions allowed by combining LEP, $R_{h \rightarrow \gamma\gamma}$ and DM direct detection constraints, for $\Lambda = 1$ TeV and $M_D = 300$ GeV for the four cases studied. Notice that case (d) is the intersection of the three other cases.

Before moving on to the calculation of the relic density, we summarize the phenomenological constraints imposed to this model by LEP χ^\pm searches, the $h \rightarrow \gamma\gamma$ decay and the direct DM detection experiments. As can be seen from Fig. 4, these constraints confine the parameters y and ξ_{12} in small regions for given M_D and the cut-off of the theory. As discussed previously, M_D is always $\gtrsim 90$ GeV which is independent of the cut-off. A general comment is that the bound imposed by the direct detection experiments in eq. (4.2) binds y and ξ_{12} together (and also forces ξ_{12} to be mostly positive).

4.4 Electroweak oblique corrections

In general, when one adds new matter into the SM particle content, with non-trivial gauge quantum numbers, severe bounds arise from the so-called oblique electroweak corrections. These loop corrections to electroweak precision observables are commonly parametrised by three parameters, S , T and U , introduced long ago in refs. [56, 57]. Even though the new matter fields \mathbf{D}_1 and \mathbf{D}_2 have common, vectorlike, mass M_D from eq. (2.1), there are mass splittings amongst the two doublets as well amongst their components themselves. These mass splittings arise from $d = 5$ operators in eq. (2.12) as discussed in the previous section.

In order to calculate the S , T and U parameters in the EFT at hand, we need to calculate vacuum polarization diagrams like the one depicted in Fig. 5, for all relevant interactions arisen from $d = 4$ and $d = 5$ operators given in section 3.2. The general form of this diagram is

$$\begin{aligned}
 i \Pi_{V_1 V_2}^{\mu\nu} = & \int d^d k \mu^\epsilon \frac{(-1)}{(2\pi)^d} \frac{1}{\left[\left(k + \frac{q}{2} \right)^2 - m_1^2 \right] \left[\left(k - \frac{q}{2} \right)^2 - m_2^2 \right]} \times \\
 & \text{Tr} \left[\left(a_{21} \gamma^\mu + \frac{b_{21}}{4\Lambda} [\not{q}, \gamma^\mu] \right) \left(\not{k} + \frac{\not{q}}{2} + m_1 \right) \left(a_{12} \gamma^\nu - \frac{b_{12}}{4\Lambda} [\not{q}, \gamma^\nu] \right) \left(\not{k} - \frac{\not{q}}{2} + m_2 \right) \right],
 \end{aligned} \tag{4.13}$$

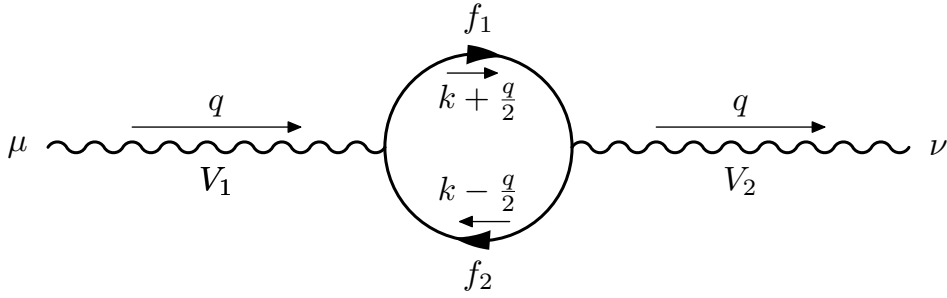


Figure 5: The Feynman diagram contributing to the oblique parameters. $V_{1,2}$ represent the gauge bosons Z, W , or γ , while $f_{1,2}$ are $\chi_{1,2}^0$ and/or χ^\pm .

where μ is the renormalization scale, $\epsilon \equiv 4 - d$, $a_{12,21}$ and $b_{12,21}$ are the gauge and the dipole couplings for every possible $\{f_{1,2}, V_{1,2}\}$ combination, where $V_{1,2}$ can be the gauge bosons Z, W , or γ and $f_{1,2}$ are $\chi_{1,2}^0$ and/or χ^\pm .

If we express the fermion masses circulating in the loop as $m_{1,2} = M_D + c_{1,2}v^2/\Lambda$ and expand eq. (4.13) up to the order $\mathcal{O}(\Lambda^{-1})$ ⁷, the term proportional to $g^{\mu\nu}$ and its derivative w.r.t. q^2 at $q^2 = 0$, read as

$$\Pi_{V_1 V_2}(q^2 = 0) = \epsilon \frac{a_{12} a_{21}}{8\pi^2 \Lambda} (c_1 + c_2) v^2 M_D \log\left(\frac{M_D^2}{\mu^2}\right) \xrightarrow{\epsilon \rightarrow 0} 0, \quad (4.14a)$$

$$\begin{aligned} \frac{d}{dq^2} \Pi_{V_1 V_2}(q^2 = 0) &= \frac{a_{12} a_{21}}{12\pi^2} \left[\log\left(\frac{M_D^2}{\mu^2}\right) + \frac{2}{\epsilon} - \gamma + \log(4\pi) \right] \\ &+ \frac{1}{48\pi^2 \Lambda M_D} \left\{ 4a_{12} a_{21} (c_1 + c_2) v^2 + 6M_D^2 (a_{21} b_{12} + a_{12} b_{21}) \left[\log\left(\frac{M_D^2}{\mu^2}\right) + \frac{2}{\epsilon} - \gamma + \log(4\pi) \right] \right\}. \end{aligned} \quad (4.14b)$$

Using these equations and substituting for every combination of $\{f_{1,2}, V_{1,2}\}$, the $a_{12}, a_{21}, b_{12}, b_{21}$ and c_1, c_2 in the expressions for the parameters S, T , and U [56], with the interactions given in section 3.2, one obtains up to terms of $\mathcal{O}(1/\Lambda^2)$, that

$$S = -\frac{2}{3\pi} \frac{v^2 y_{12}}{\Lambda M_D}, \quad T = 0, \quad U = 0. \quad (4.15a)$$

These results have been checked independently using the analytical expressions of ref. [18] and interactions from section 3.2 keeping terms up to $1/\Lambda$. In addition, they have been verified numerically by taking the decoupling limit of the fermion triplet mass $M_T \gg M_D$ in ref. [18].

The parameter S measures the size of the new fermion sector *i.e.*, the number of the extra $SU(2)_L$ irreducible representations that have been added in the model. In general, the contribution of degenerate fermions to the S -parameter is

$$S \sim \sum_{\text{new fermions}} (T_{(R)}^3 - T_{(L)}^3), \quad (4.16)$$

⁷ By doing so, one avoids the introduction of involved $d = 6$ operators. Their inclusion would lead to weak bounds on the corresponding Wilson coefficients (a related discussion can be found in ref. [58]).

where $T_{(L,R)}^3$ is the isospin of the left- and right-handed fermions. So, in a case similar to ours, where the fermions are nearly degenerate, the S -parameter takes the form

$$S \sim \sum_{\text{new fermions}} (T_{(R)}^3 - T_{(L)}^3) + f(m_{\chi_1^0}, m_{\chi_2^0}, m_{\chi^+}), \quad (4.17)$$

where $f(m_{\chi_1^0}, m_{\chi_2^0}, m_{\chi^+})$ is a function that vanishes if the three masses are equal. Therefore, in our case, the S -parameter for two vector-like doublets would arise only from the mass differences, which means that S -parameter is proportional to the Yukawa couplings⁸. After performing the calculation, it turns out that

$$f(m_{\chi_1^0}, m_{\chi_2^0}, m_{\chi^+}) \propto \frac{\Delta m_{1^+} + \Delta m_{2^+}}{M_D}, \quad (4.18)$$

where $\Delta m_{i^+} \equiv m_{\chi_i^0} - m_{\chi^\pm}$. This is proportional to y_{12} , as can be seen in eq. (4.15a). Furthermore, no magnetic dipole parameters d_γ or d_W are involved in S -parameter in (4.15a) up to $\mathcal{O}(1/\Lambda^2)$, as also expected from dimensional arguments.

The U -parameter, on the other hand, measures the size of the isospin breaking contribution from the new fermions. So, it should be suppressed due to the c.c. (or custodial) symmetry (which limits the isospin breaking) and the fact that we are keeping only terms up to $1/\Lambda$. Up to this order, the parameter T is zero too, because $\Pi_{V_1 V_2}(q^2 = 0) = 0$, a result which is independent of the symmetric limits for y_{12} . Usually, the parameters T and U are proportional to the ratio $\frac{\Delta m^2}{M_Z^2 \text{ or } M_D^2}$, where Δm^2 is some mass-squared difference arising from isospin breaking. In our model this should be the case when $y \neq 0$ and $y_{12} \neq 0$, which means that higher order terms could give a non-vanishing (but suppressed by terms $\propto \Lambda^{-2}$) contribution. Experimentally, S, T and U -parameters fit the electroweak data for $U = 0$ with values [6]:

$$S = 0.00 \pm 0.08, \quad T = 0.05 \pm 0.07. \quad (4.19)$$

In Fig. 6, we present a contour plot for the S -parameter obtained from (4.15) as a function of y_{12} and M_D for $\Lambda = 1$ TeV. As expected, stronger (1σ) bounds from eq. (4.19) are obtained in the region $M_D \approx 100$ GeV, where it must be $|y_{12}| \lesssim 1$. On the other hand, relaxed bounds on $|y_{12}|$ are obtained for higher values of M_D and/or Λ .

Apparently the result of eq. (4.15a), does not interfere with the bounds discussed before for the cases (b) and (c), since the allowed values of y_{12} , obtained from (4.19), are equivalent to those obtained by the combination of the DM direct searches, the $h \rightarrow \gamma\gamma$ decay and LEP χ^\pm bounds. On the contrary, in case (a) where $y = y_{12}$, the bounds on y arise only from the S -parameter.

5 Cosmological and astrophysical constraints

In the context of this model, it is essential to calculate the DM relic density Ωh^2 of the dark fermion χ_1^0 , in order to impose the cosmological constraint related to the Planck satellite

⁸The coupling ξ_{12} is just a universal shift to M_D and thus it does not contribute to the mass difference. Also, as it turns out, y does not appear in $\frac{d}{dq^2} \Pi_{V_1 V_2}(q^2 = 0)$ (for every V_1 and V_2 combination). Only y_{12} contributes to the oblique EW parameters at the approximation in $1/\Lambda$.

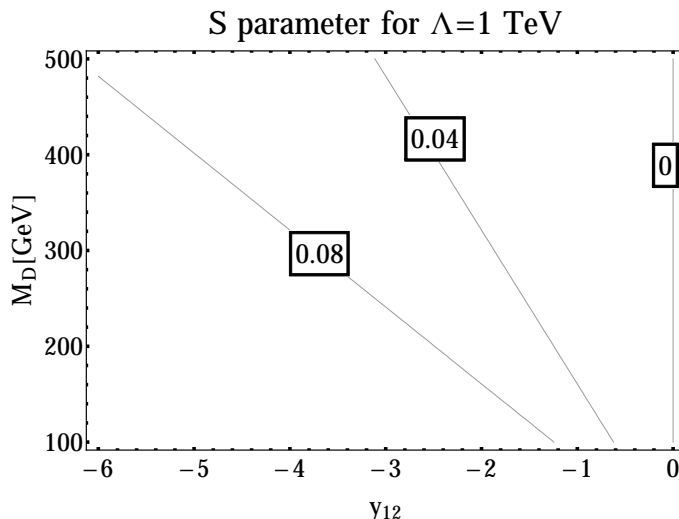


Figure 6: *Contours of the S-parameter on $y_{12} - M_D$ plane for $\Lambda = 1$ TeV.*

measurements [6], as expressed in eq. (1.1). Assuming that χ_1^0 constitutes the DM of the universe, we are able to set severe constraints on the parameters of eq. (2.17), in conjunction to those found previously in section 4. From now on we focus on benchmark cases (b) and (c) mainly because there is more freedom move around the parameter space as compared to cases (a) and (d).

In this section we describe briefly the freeze-out mechanism and discuss the solution of the Boltzmann equation. Afterwards, we present general, analytical, predictions for Ωh^2 , aiming to understand its dependences, and then numerical solutions are discussed. Additionally, we study the constraints imposed by the gamma fluxes produced by DM annihilations in the galactic center (GC) [59, 60] and in various dwarf spheroidal satellite galaxies (dSph) [61]. Finally, at the end of this section, we briefly discuss neutrino fluxes from the Sun, which are constrained from IceCube experiment [62, 63].

5.1 Dark Matter relic abundance

The conventional way to produce non-relativistic (cold) DM relic particle abundance, is the so called freeze-out mechanism [64, 65]. Although this mechanism is well reviewed in the literature [3, 66–70], it would be helpful to outline the main steps here.

In the early universe, when the temperature was much higher than M_D , the would-be DM particles were in equilibrium, which means that it was equally possible to create and destroy pairs of them due to the Z_2 -symmetry. As temperature of the universe was dropping, the thermal production of DM pairs became inefficient. Thus, χ_1^0 pairs started to annihilate into lighter SM particles. As the number of these would-be DM particles was dropping, it became increasingly rare for them to interact with each other and annihilate. This yielded an almost constant number density of χ_1^0 particles, which corresponds to DM relic density observed today.

Assuming that χ_1^0 is the lighter particle of the dark sector, one can evaluate the relic

density accurately⁹ by solving the corresponding Boltzmann equation:

$$\frac{dn_{\chi_1^0}}{dt} + 3Hn_{\chi_1^0} = -\langle\sigma v_{rel}\rangle\left(n_{\chi_1^0}^2 - n_{\chi_1^0}^{(eq)2}\right), \quad (5.1)$$

where H is the Hubble parameter defined as

$$H \equiv \frac{\dot{\alpha}(t)}{\alpha(t)}, \quad (5.2)$$

and $\alpha(t)$ is the cosmic scale factor. Also $n_{\chi_1^0}$ is the WIMP number density and $n_{\chi_1^0}^{(eq)}$ is the corresponding quantity in equilibrium

$$n_{\chi_1^0}^{(eq)} \equiv g \left(\frac{m_{\chi_1^0} T}{2\pi}\right)^{3/2} e^{-x}, \quad x \equiv \frac{m_{\chi_1^0}}{T}, \quad (5.3)$$

where g is the number of the internal degrees of freedom of a particle, $\langle\sigma v_{rel}\rangle$ is the thermal average of the total annihilation cross-section of the WIMP to all allowed particles (k, l), multiplied by the relative velocity of the incoming particles, which is usually expanded as

$$\langle\sigma v_{rel}\rangle = \sum_{k,l} \left\langle\sigma_{\chi_1^0\chi_1^0 \rightarrow k,l} v_{rel}\right\rangle = a + b \langle v_{rel}^2 \rangle + \dots \quad (5.4)$$

It should be noted, that the second term on the r.h.s. of eq. (5.1) is responsible for creating χ_1^0 -pairs, while the first term for annihilating them. According to our description above, at high temperatures, much higher than $m_{\chi_1^0}$, the r.h.s of eq. (5.1) vanishes. This results to a constant particle number density since

$$\frac{dn_{\chi_1^0}}{dt} + 3Hn_{\chi_1^0} = \frac{1}{\alpha^3} \frac{d(\alpha^3 n_{\chi_1^0})}{dt} = 0. \quad (5.5)$$

For lower temperatures than $m_{\chi_1^0}$, the term $\langle\sigma v_{rel}\rangle n_{\chi_1^0}^{(eq)2}$ in eq. (5.1) should vanish, since the WIMP pairs are not produced effectively [see eq. (5.3)]. Then the Boltzmann equation can be approximated as

$$\frac{dn_{\chi_1^0}}{dt} \approx -\left(\langle\sigma v_{rel}\rangle n_{\chi_1^0} + 3H\right) n_{\chi_1^0}. \quad (5.6)$$

The freeze-out temperature is defined as this where the annihilation rate becomes comparable to the expansion rate of the universe

$$\langle\sigma v_{rel}\rangle n_{\chi_1^0} \approx H. \quad (5.7)$$

The freeze-out temperature T_f can be evaluated iteratively, through

$$x_f = \log \left[c(c+2) \sqrt{\frac{45}{8}} \frac{m_{\chi_1^0} M_P (a + 6b/x_f)}{g_\star^{1/2} x_f^{1/2}} \right], \quad (5.8)$$

where $x_f \equiv m_{\chi_1^0}/T_f$. The parameter c is usually chosen $c \sim 0.5$, to get into agreement with precise numerical solutions of the Boltzmann equation. Furthermore, $M_P \approx 2.435 \times 10^{18}$ GeV

⁹Extensive discussion on the solution of the Boltzmann equation including coannihilation effects can be found in [71].

is the Planck scale, and g_* counts the relativistic degrees of freedom of the Standard Model at $T_f = m_{\chi_1^0}/x_f$. It turns out that $x_f \simeq 25$. Calculating the freeze-out temperature, one can solve the Boltzmann equation and find the present WIMP relic density

$$\Omega h^2 \approx \frac{1.04 \times 10^9 \text{ GeV}^{-1}}{M_P} \frac{x_f}{g_*^{1/2}(a + 3b x_f^{-1})}. \quad (5.9)$$

For a WIMP mass at the electroweak scale, this formula becomes approximately $\Omega h^2 \approx 0.1 \frac{10^{-8} \text{ GeV}^{-2}}{a+3b x_f^{-1}}$. From eq. (1.1) we get $\Omega h^2 \sim 0.1$, so the required cross-section is of order 10^{-8} GeV^{-2} for $a = \mathcal{O}(\text{GeV}^{-2})$, which is a typical EW cross section.

If other particles are almost degenerate with WIMP, then there could be extra contributions (coannihilation effects) to the total annihilation cross-section due to them. Thus, the annihilation cross-section modified in order to incorporate these coannihilation effects [72]. Following [66, 72], this change is

$$\sum_{k,l} \sigma_{\chi_1^0 \chi_1^0 \rightarrow k,l} \rightarrow \sigma_{eff} = \sum_{k,l} \sum_{i,j} \sigma_{i,j \rightarrow k,l} \frac{g_i g_j}{g_{eff}^2(x)} (1 + \Delta_i)^{3/2} (1 + \Delta_j)^{3/2} e^{-x(\Delta_i + \Delta_j)}, \quad (5.10)$$

where indices i, j run over all the co-annihilating particles with $\Delta_i = \frac{m_i - m_{\chi_1^0}}{m_{\chi_1^0}} \lesssim 0.1$ and $g_{eff}(x)$ is defined as

$$g_{eff}(x) \equiv \sum_i g_i (1 + \Delta_i)^{3/2} e^{-x\Delta_i}. \quad (5.11)$$

Such coannihilation effects, and other possible contributions to the relic abundance [72], have been included in our numerical analysis described in the following.

5.2 A close look at the relic density

Before discussing the bounds imposed by the data on Ωh^2 , it would be helpful to study the numerical values of the annihilation cross-section that are used to calculate the relic abundance. As discussed in section 4.3, if $M_D \gtrsim 90 \text{ GeV}$, then the coupling to the Higgs boson is approximately zero. Therefore, the most important annihilation channels, assuming for the time being that coannihilation effects are irrelevant, are $\chi_1^0 \chi_1^0 \rightarrow W^+ W^-, ZZ, \gamma Z$ and $\gamma\gamma$. There are no final states with fermions, since their corresponding interaction vertices are absent. There are no $\chi_1^0 \chi_1^0 Z/\gamma$ terms in the Lagrangian of eqs. (3.13) and (3.17), or they are restricted because of bounds by direct detection experiments $Y^{h\chi_1^0 \chi_1^0} \approx 0$.

Keeping only the first term in the expansion of eq. (5.4) we obtain

$$a_{VV} = \frac{\beta_V^{3/2} m_{\chi_1^0}^2}{32\pi S_V v^2} \frac{\left[g^2 v^4 - 4g v^2 \omega K_V (m_{\chi_1^0} + m_\chi) + 4K_V^2 \omega^2 (2m_{\chi_1^0} m_\chi + M_V^2) \right]^2}{v^6 (m_{\chi_1^0}^2 + m_\chi^2 - M_V^2)^2}, \quad (5.12)$$

where V denotes W and Z gauge bosons in the final states for the processes $\chi_1^0 \chi_1^0 \rightarrow W^+ W^-$ or $\chi_1^0 \chi_1^0 \rightarrow ZZ$. Also, we abbreviate, $\beta_V \equiv 1 - M_V^2/m_{\chi_1^0}^2$, $K_W \equiv d_W$, $S_W \equiv 1$, $K_Z \equiv c_W(c_W d_W + s_W d_\gamma)$ and $S_Z \equiv 2c_W^4$. The mass m_χ denotes m_{χ^\pm} for $V = W$ and $m_{\chi_2^0}$ for $V = Z$.

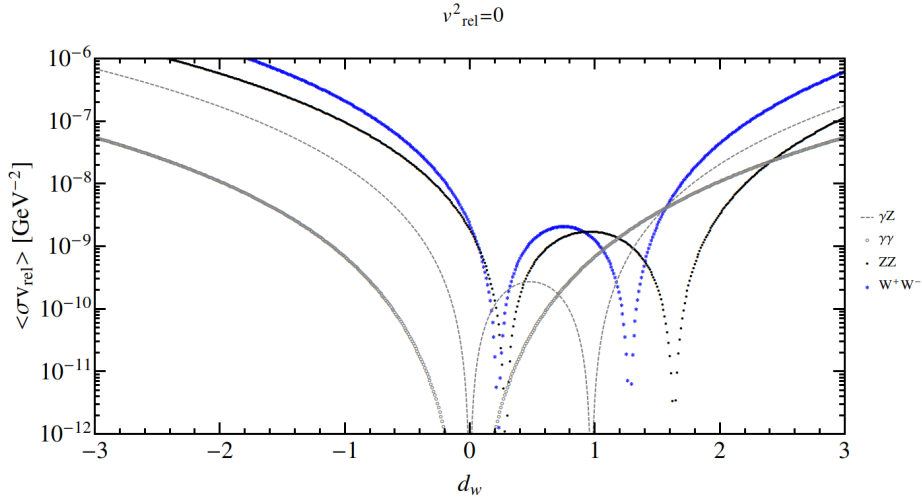


Figure 7: The dependence of different annihilation channels on d_W for $M_D = 400$ GeV, $\Lambda = 1$ TeV, $y = -y_{12} = -\frac{\xi_{12}}{2} = -0.8$ and $d_\gamma = 0$. Notice that, in a certain range of d_W values, there is at least one dip for each channel cross section.

For the channels γZ and $\gamma\gamma$, we find

$$a_{\gamma Z} = \frac{\beta_{\gamma Z}^3 m_{\chi_1^0}^2 C_\gamma^2 \omega^2 \left[g v^2 (m_{\chi_1^0} + m_{\chi_2^0}) - \omega K_Z (4m_{\chi_1^0} m_{\chi_2^0} + M_Z^2) \right]^2}{2\pi c_W^2 v^2 v^6 \left[2(m_{\chi_1^0}^2 + m_{\chi_2^0}^2) - M_Z^2 \right]^2}, \quad (5.13a)$$

$$a_{\gamma\gamma} = \frac{m_{\chi_1^0}^4 m_{\chi_2^0}^2 \omega^4 C_\gamma^4}{\pi (m_{\chi_1^0}^2 + m_{\chi_2^0}^2)^2 v^8}, \quad (5.13b)$$

with $\beta_{\gamma Z} \equiv 1 - M_Z^2/4m_{\chi_1^0}^2$ and $C_\gamma \equiv (c_W d_\gamma - s_W d_W)$. These channels $\gamma\gamma$ and γZ , contribute to the monochromatic gamma fluxes from the GC. Thus, in conjunction to the corresponding bounds from Fermi-LAT experiment, one gets severe constraints for the coupling C_γ . Due to absence of χ_1^0 couplings to Z and γ and the nearly vanishing Higgs mediated \hat{s} -channel, all the above processes arise from \hat{t} and \hat{u} channels.

Eqs. (5.12), (5.13a) and (5.13b), contain one or more solutions with respect to d_W . This means that d_W could act as a regulator that minimizes the total annihilation cross-section as the (required) low mass M_D tends to amplify it (generally the cross section scales as M_D^{-2} if we ignore magnetic dipole interactions). This minimization, will be proved essential when trying to obtain cosmologically acceptable relic abundance at the electroweak scale.

Qualitatively, concerning the minimum of the *total* annihilation cross-section as a function of the dipole couplings one anticipates that each cross-section should be minimized for almost the same value of d_W , in order for the *total* annihilation cross-section to be at its minimum. In addition, $d_\gamma \approx \frac{s_W}{c_W} d_W$ so that C_γ is quite small. This keeps d_γ from obtaining large negative values, because a_{WW} can be minimized only for $d_W > 0$.

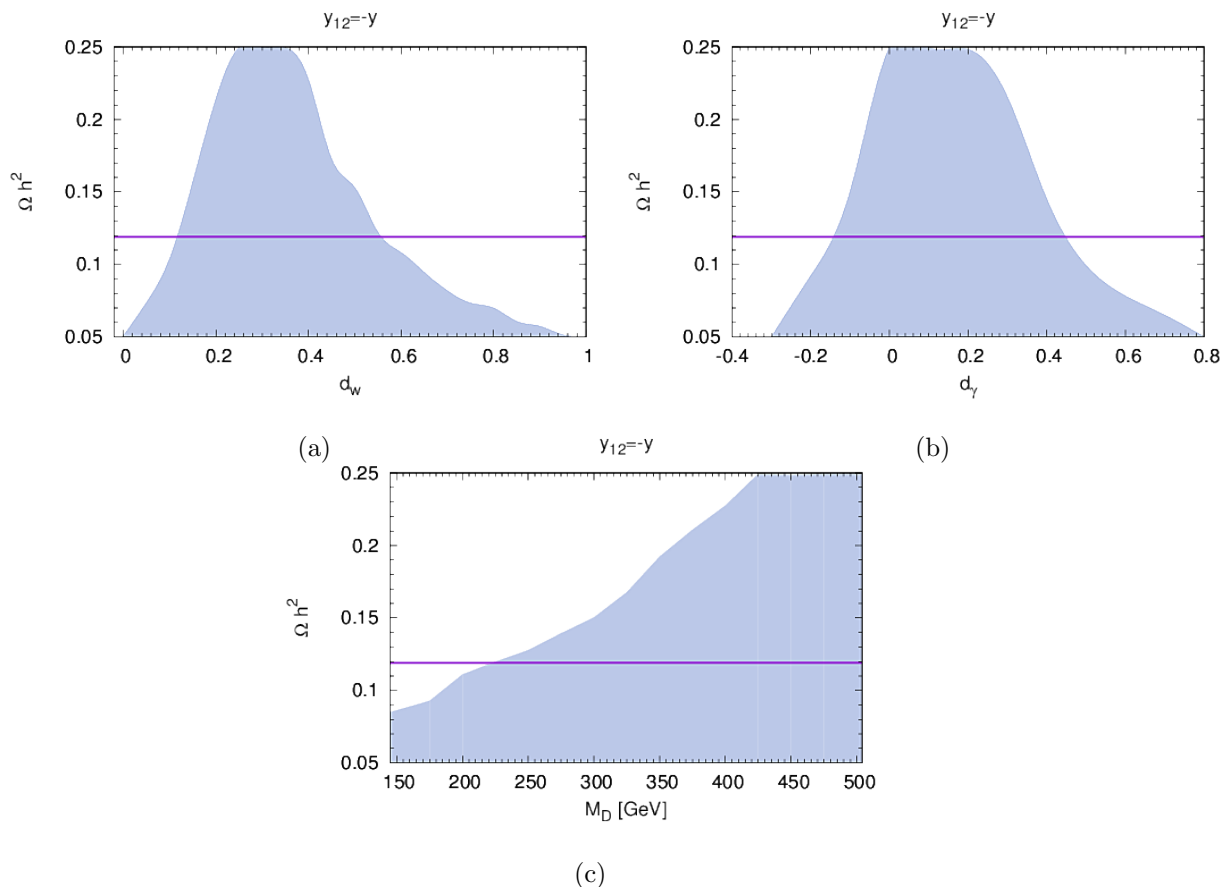


Figure 8: *Relic abundance dependence on the parameters (a) d_W , (b) d_γ , and (c) M_D , for $\Lambda = 1$ TeV and $y_{12} = -y$. The cosmologically allowed (shaded) region corresponds to the variation of the other parameters in (2.17) not shown in the plot. The horizontal line stands for $\Omega h^2 = 0.12$.*

A numerical example is shown in Fig. 7. We observe that there are two minima for the annihilation cross-sections to ZZ , W^+W^- and γZ and one minimum for $\gamma\gamma$. The first minimum of a_{ZZ} and a_{WW} coincides with the vanishing point of C_γ , which gives small cross-sections for $\chi_1^0\chi_1^0 \rightarrow \gamma\gamma$ and γZ . On the other hand, the second minimum of a_{ZZ} and a_{WW} is in a region where the annihilation to $\gamma\gamma$ and γZ blows up. Furthermore, for negative d_W , there are no such minima and, as can be seen from Fig. 7, every cross-section becomes quite large.

Since eq. (5.9) is an approximation which could lead to an error up to $\sim 10\%$ (as discussed in ref. [72]), the Boltzmann equation must be solved numerically. To do this we implement the $d = 4$ and $d = 5$ operators to the computer program microOMEGAs [73] via the LanHEP [74] package¹⁰ in order to obtain more accurate results for the relic abundance.

In Figs. 8a, 8b and 8c we examine the dependence of the relic abundance Ωh^2 on the parameters, d_W , d_γ and M_D , respectively. Because all parameters in (2.17), run freely, the

¹⁰More information about these packages can be found in <https://laph.cnrs.fr/micromegas/> and <http://theory.sinp.msu.ru/~semenov/lanhep.html>.

corresponding plots are given as shaded areas in Fig. 8. We remark that: *a)* The minimization effects on the various cross-sections discussed before, are evident in the numerical results too. *b)* As expected, when M_D increases, Ωh^2 increases too. *c)* For acceptable Ωh^2 and M_D of a few hundred GeV, d_W must lie in the region $0.1 \lesssim d_W \lesssim 0.5$, which does not include the zero node. The dipole moment to photon d_γ should be in the region $-0.2 \lesssim d_\gamma \lesssim 0.5$, which includes the zero node. *d)* The minimization of the total annihilation cross-section, is not enough to produce the observed DM density for $M_D \lesssim 200$ GeV.

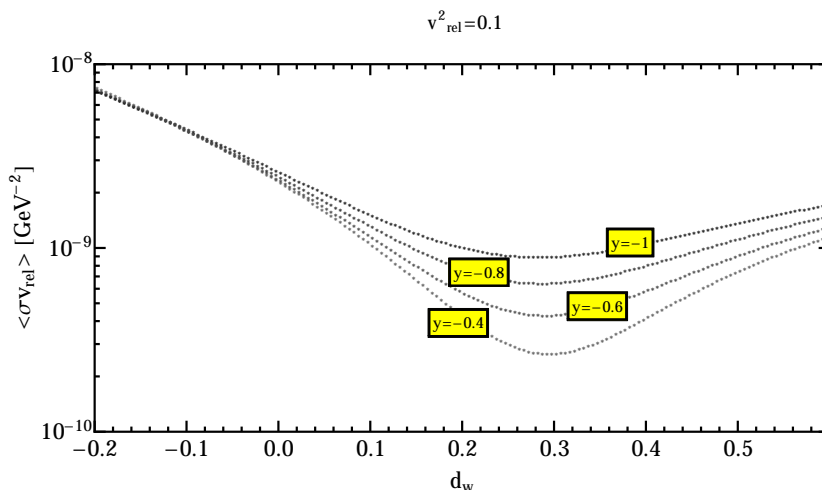


Figure 9: ZZ annihilation cross section dependence on d_W for different values of $y = -y_{12} = -\frac{\xi_{12}}{2}$, $\Lambda = 1$ TeV, $M_D = 400$ GeV, $d_\gamma = 0$ and $v_{\text{rel}}^2 = 0.1$. At the minimum, the values of the cross-section decreases as we lower the values of $|y|$. The behaviour of the W^+W^- annihilation channel is similar.

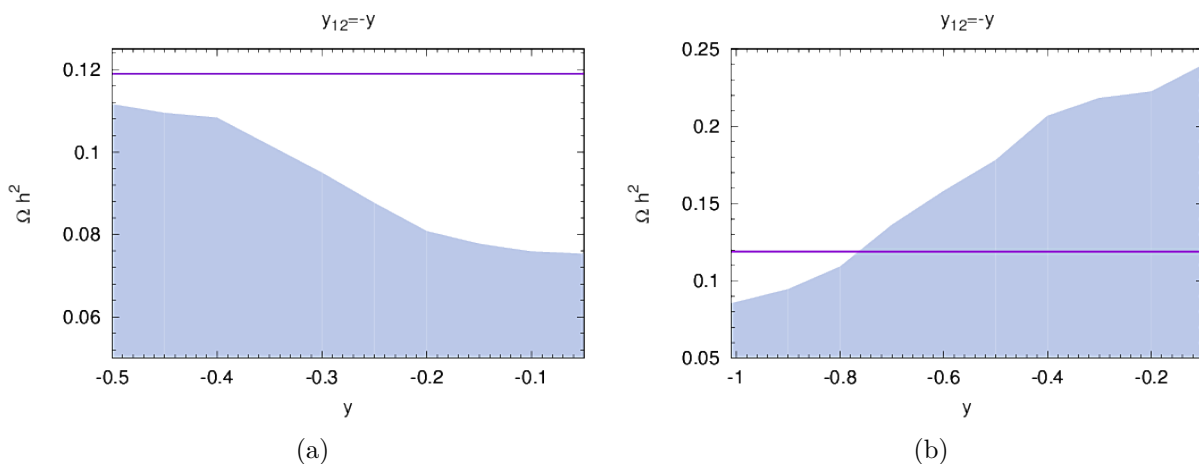


Figure 10: y vs. Ωh^2 , for $\Lambda = 1$ TeV and (a) $M_D = 200$ GeV and (b) $M_D = 400$ GeV. Other parameters from the list (2.17) vary in the range constrained from “Earth” constraints and for $y_{12} = -y$. The dependence of the relic density on y changes for different values of M_D .

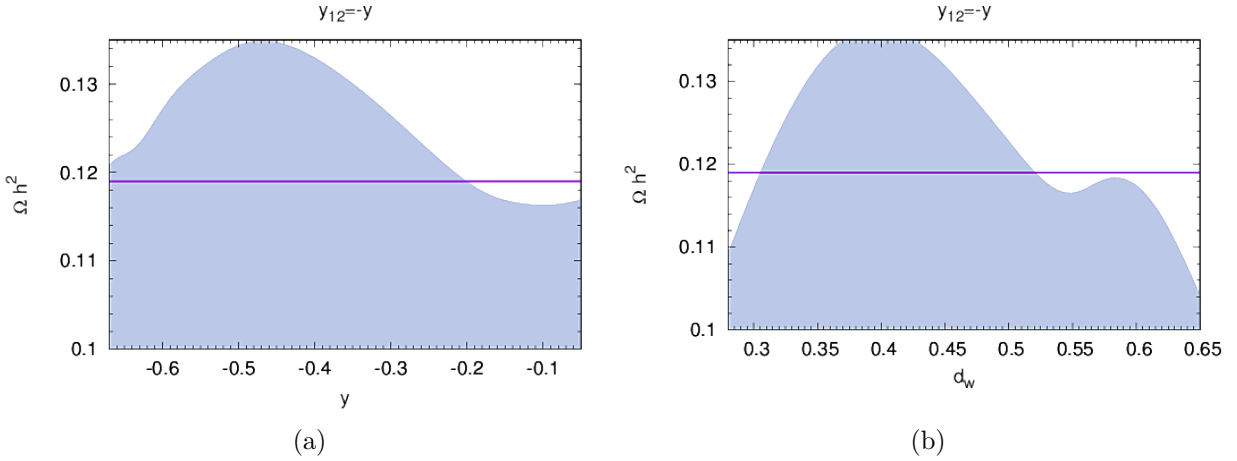


Figure 11: *Turning point as can be seen in (a) y versus Ωh^2 and (b) d_W versus Ωh^2 , for $y_{12} = -y$, $\Lambda = 1$ TeV and $M_D = 260$ GeV. The shaded area and the curves are as in Fig. 8.*

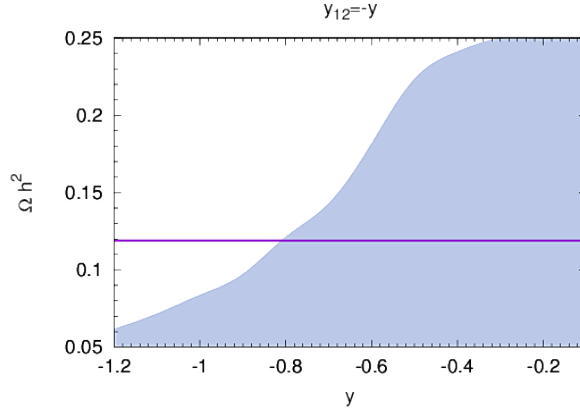


Figure 12: *Ωh^2 versus y , for $y_{12} = -y$, $\Lambda = 1$ TeV and $M_D \leq 500$ GeV. The shaded area and the curves are as in Fig. 8.*

The dependence of the relic density on the parameter y is complicated due to the following competing effects: The coannihilation channels, increase the total annihilation cross-section as $|y|$ tends to zero, since the mass differences of the initial particles involved become smaller and smaller. But, as shown in Fig. 9, the b -term in the expansion of eq. (5.4), tends to decrease the value of the cross-sections (around the minimum), at least for the annihilation to ZZ and W^+W^- .

Moreover, in Fig. 10 we study the dependence of Ωh^2 on y , for various values of the mass M_D . In the region $M_D \lesssim 260$ GeV, the relic abundance becomes smaller for smaller y (an example for $M_D = 200$ GeV is shown in Fig.10a), which means that the coannihilation effects dominate over the b -term, and vice-versa for larger values of M_D (Fig.10b).

There is a small region at $M_D \approx 260$ GeV where this dependence is mixed. We call this value of M_D “turning point”. An example of this behavior is shown in Fig.11a. As we can see, the relic abundance rises until $y \sim -0.4$ and then decreases, but for $y \sim -0.06$ it starts to increase again. Also, as shown in Fig.11b, we obtain two maxima for Ωh^2 with respect to d_W ,

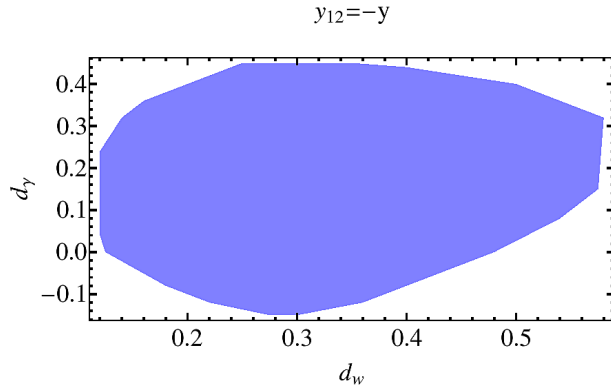


Figure 13: The plane $d_W - d_\gamma$ of the parameter space that gives the observable relic abundance, for $\Lambda = 1$ TeV and $y_{12} = -y$. The same region holds also for $y_{12} = 0$. We allow variation of other parameters in (2.17) consistently with observational data.

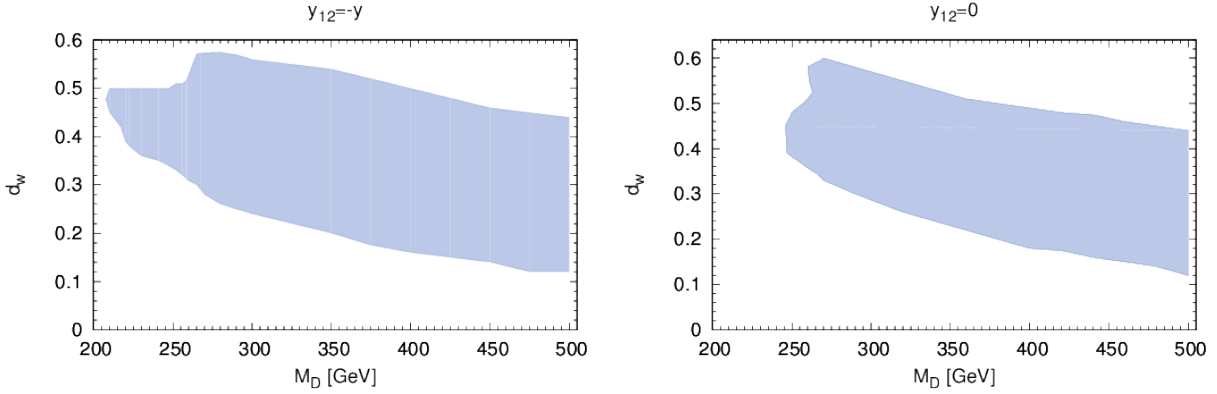
as a result of this effect, since the value of d_W which minimizes the annihilation cross-section depends on y .

Although y has no definite effect on Ωh^2 , the relic density increases as M_D increases. Therefore, if we calculate the relic density in the allowed parameter space, the dependence of the relic on y would be dominated by its dependence for larger M_D . In Fig. 12, we show the dependence of Ωh^2 on y . The relic density decreases as $|y|$ becomes larger and for $|y| \gtrsim 0.9$ the DM becomes under-abundant.

Finally, the case where $y_{12} = 0$ yields similar results with the case $y_{12} = -y$ just discussed, as can be deduced from Figs. 8 and 12. Also, for other values of the cut-off scale Λ , the parameters $d_{\gamma, W}$ and y should be rescaled in order for the ratios d_W/Λ , d_γ/Λ and y/Λ to remain unchanged.

5.3 Cosmological constraints due to relic density

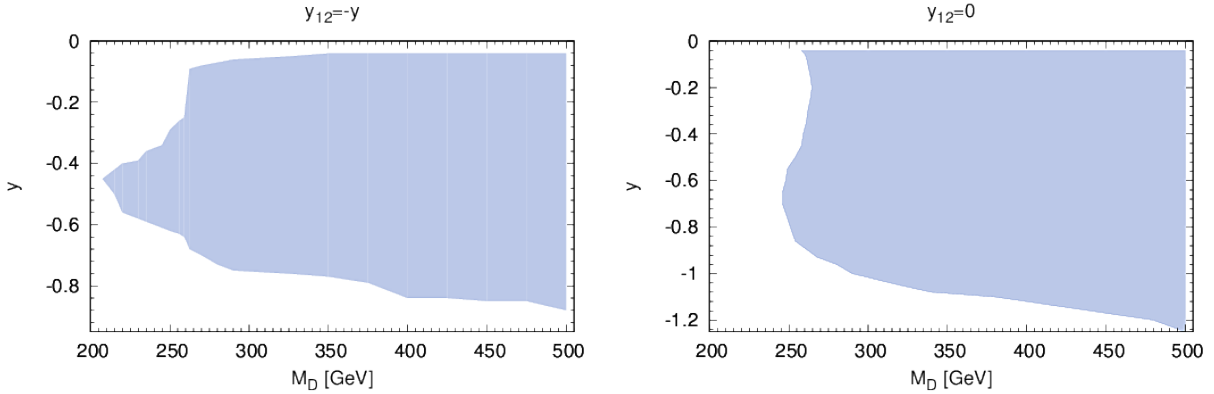
Having studied the constraints from LEP , $R_{h \rightarrow \gamma\gamma}$, the direct detection DM experiments as well as the Planck bound on the relic density for this effective theory, we are able delineate the cosmologically acceptable regions of the parameter space. For this reason, we perform a combined scan in the so far allowed parameter space which is also cosmologically preferred, for the cases $y_{12} = -y$ and $y_{12} = 0$ at $\Lambda = 1$ TeV. First, for $\Lambda = 1$ TeV, in Fig. 13 we display the part of the $d_\gamma - d_W$ plane, that is compatible to the DM relic density, varying all the other parameters, but keeping $M_D \lesssim 500$ GeV. Apparently the parameter d_W is bounded to be positive in order to explain the DM relic abundance for a WIMP mass at electroweak scale. Also, the region where d_γ is positive, is larger than the region where it is negative, a situation explained in the preceding analysis. A similar region is also found for $y_{12} = -y$ and $y_{12} = 0$.



(a) M_D vs d_W , for $\Lambda = 1$ TeV and $y_{12} = -y$.

(b) M_D vs d_W , for $\Lambda = 1$ TeV and $y_{12} = 0$.

Figure 14: As in Fig. 13 but for acceptable values on the plane $M_D - d_W$.



(a) M_D vs y , for $\Lambda = 1$ TeV and $y_{12} = -y$.

(b) M_D vs y , for $\Lambda = 1$ TeV and $y_{12} = 0$.

Figure 15: Values on $M_D - y$ plane that provide acceptable DM relic abundance.

In Fig. 14 we observe that M_D vastly affects the allowed values for d_W that provide the correct relic abundance. This is due to the fact that the minimum of the total annihilation cross-section depends on the mass M_D , as can be seen from eqs. (5.12), (5.13a) and (5.13b) and also from the fact that the maximum of Ωh^2 varies as M_D changes, see also Fig. 8c. Moreover, as M_D becomes larger, the minimization of the cross-section becomes less necessary. Note that, for $y_{12} = 0$ there is a gap for d_W at $M_D \approx 260$ GeV, a result of the “turning point” discussed at the end of the previous paragraph (see Fig. 11b). For $y_{12} = -y$, this “turning point” is ineffective.

In Fig. 15 one can see the dependence of M_D on y , in the region where the DM density complies the current cosmological bound. We observe that for large values of M_D , for $|y| < 0.85(1.25)$ for the case $y_{12} = -y$ ($y_{12} = 0$) we obtain the desired Ωh^2 . On the contrary, when $M_D \lesssim 300$ GeV in both cases for y_{12} , $|y|$ seems to be strongly dependent on M_D . This happens because the bound on $|y|$ from Earth-based experiments becomes stronger than the one from the relic abundance for smaller masses. In addition to that, since Ωh^2 tends to

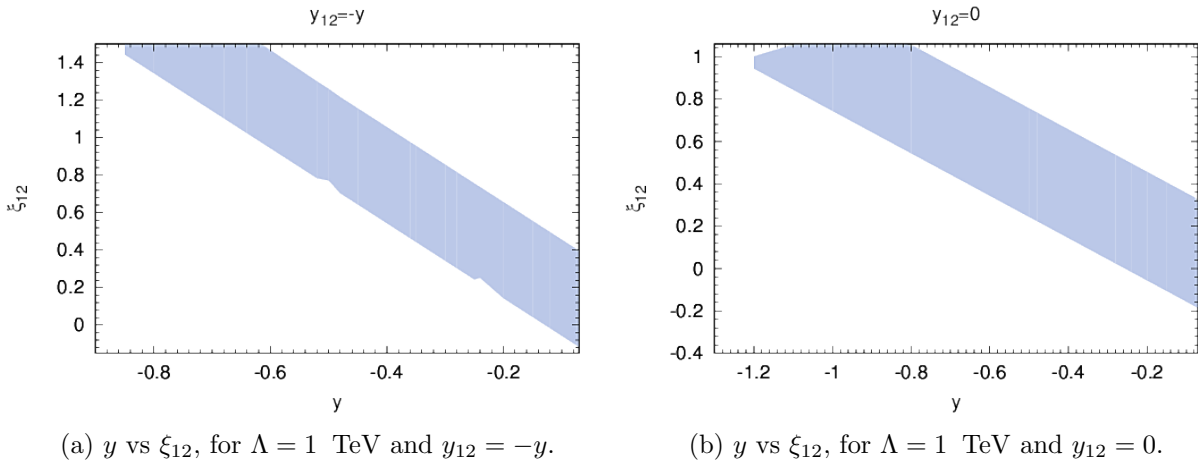


Figure 16: As in Fig. 15, but for the Yukawa parameters $y - \xi_{12}$.

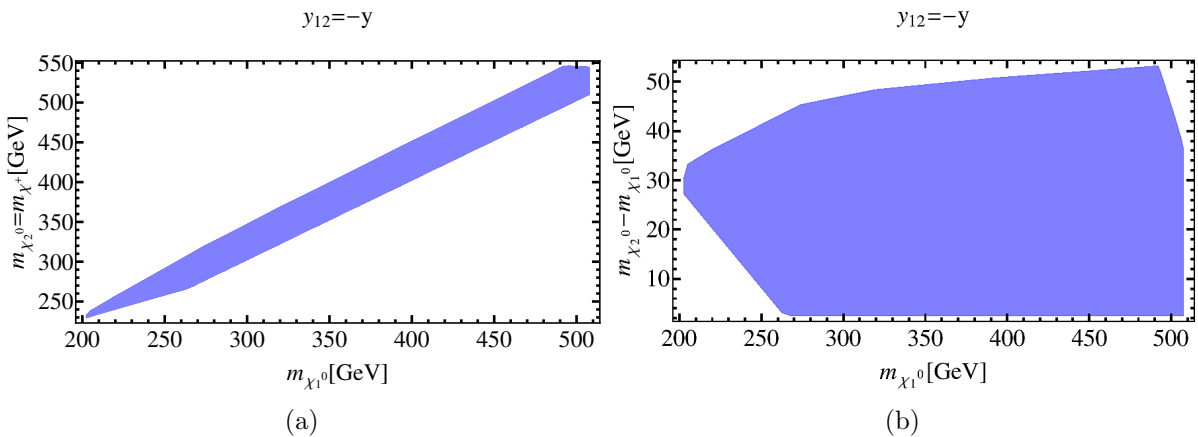


Figure 17: (a) The cosmologically allowed mass of the WIMP versus the mass of the heavy fermions and (b) their mass difference for $y_{12} = -y$. Similar regions can be obtained for $y_{12} = 0$.

decrease as $|y|$ becomes smaller for $M_D \lesssim 260$ GeV, $|y|$ is also bounded from below. Furthermore, due to the “oscillation” of the relic abundance (Fig. 11a), at $M_D \sim 260$ GeV there is a “gap” on the allowed values of y (similar to d_W). Additionally, in Fig. 16, we see that ξ_{12} follows y , a remaining result from the direct detection bound (similar to Fig. 2).

The Yukawa couplings and the mass parameter M_D displayed, fix the masses and their differences. For the sake of completeness, the masses and their difference from $m_{\chi_1^0}$ are shown in Fig. 17 for $y_{12} = -y$ (similar region holds also for $y_{12} = 0$). We observe that $m_{\chi_1^0} \gtrsim 200$ GeV, for $y_{12} = -y$, which is also what one should expect from Fig. 15. In addition to this, the mass difference $m_{\chi_2^0} - m_{\chi_1^0}$ is in the region $\sim 2 - 50$ GeV. Finally, we note that this mass difference takes slightly larger values ($\sim 2 - 70$ GeV) for the other case of the symmetric limit for y_{12} , while $m_{\chi_{\pm}} - m_{\chi_1^0}$ is always half that [see eq. (3.3)]. Accordingly, the smallest possible mass of the WIMP in this case is ~ 250 GeV (which again can be seen also from Fig. 15).

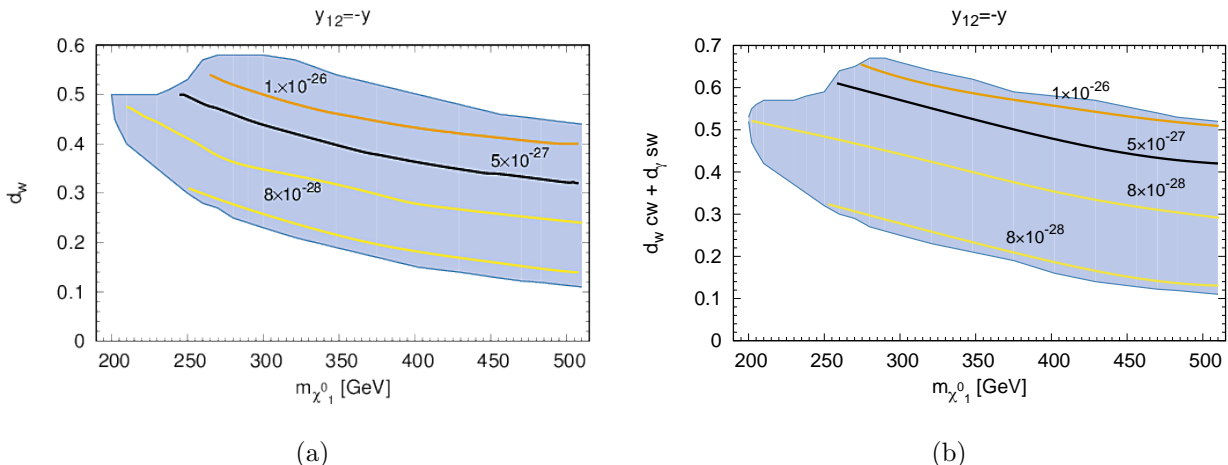


Figure 18: Allowed region in the parameter space from collider, DM direct detection and relic density constraints discussed in sections 4 and 5.3, respectively, as a function of the WIMP mass and the couplings d_W and K_Z/c_W . The contours show the values of the thermally averaged cross-sections (a) for a_{WW} and (b) for a_{ZZ} in cm^3s^{-1} for $y_{12} = -y$. Similar for $y_{12} = 0$. We take $\Lambda = 1$ TeV.

5.4 Gamma-rays

Having delineated the cosmologically acceptable regions concerning the DM abundance, we will proceed calculating other astrophysical observables, like the gamma-ray fluxes (monochromatic and continuous) originating from the Milky Way GC and dSphs.

5.4.1 Continuous Gamma spectrum

In our model the DM pair annihilation cross-sections have been studied in section 5.2. In particular, the relevant relations can be found in eq. (5.12). From refs. [61, 75] we observe that the bounds on the cross sections a_{ZZ} and a_{WW} are above the required $\sim 3 \times 10^{-26} \text{ cm}^3\text{s}^{-1}$ (for masses above 200 GeV) which generally gives the desired relic abundance. More precisely, for $m_{\chi_1^0} \gtrsim 200$ GeV, the bound from dSphs is below $\sim 5 \times 10^{-26} \text{ cm}^3\text{s}^{-1}$ for the annihilation $\chi_1^0 \chi_1^0 \rightarrow W^+W^+$ (assuming that the branching ratio is 100%). The same bound holds the annihilation to a pair of Z -bosons, since their gamma spectra are quite similar. When applied to our model, which generally gives smaller branching ratios, these bounds should be even weaker. As it is shown in Fig. 18, the relevant to continuous emission of photons cross-sections, $\sigma_{\chi_1^0 \chi_1^0 \rightarrow W^+W^-, ZZ}$ are safe with experimental bounds from continuous gamma ray spectrum discussed in this paragraph.

5.4.2 Constraints from Gamma-ray monochromatic spectrum

As we have seen, this effective theory relies on the various WIMPs magnetic dipole moment operators in order to give us the observed relic abundance. This could result to annihilations of pairs of WIMPs into photons which could be detectable from observations of gamma ray monochromatic spectrum originated from the GC. In this paragraph, we will calculate the

cross-sections for processes that could give such gamma rays (eqs. (5.13a) and (5.13b)). As input, we use the parameter space that evade all the other, previously examined, bounds and use the results from Fermi-LAT [59, 60] to set additional bounds to the parameters of this model.

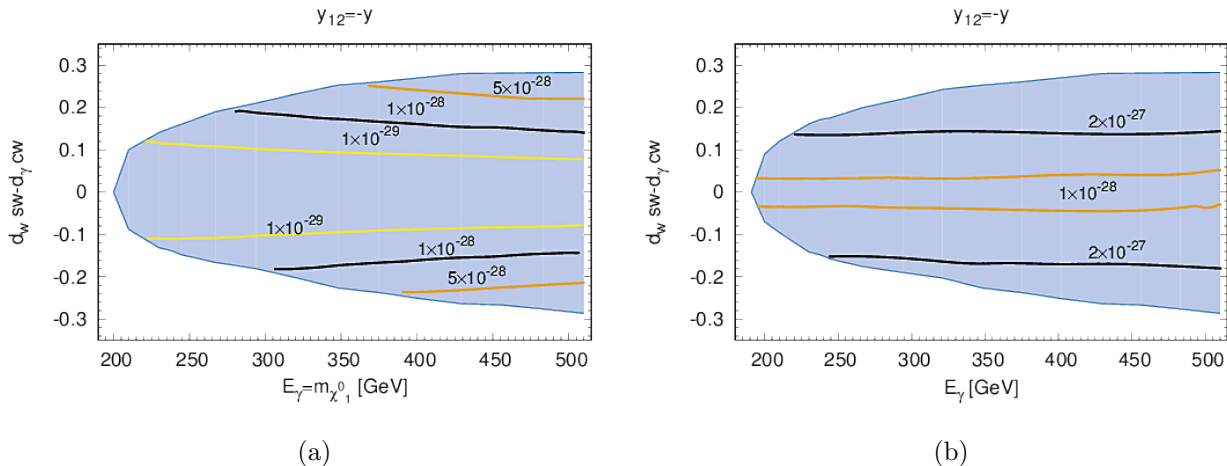


Figure 19: The allowed, as in Fig. 18, region of the parameter space, in terms of the photon energy and the coupling C_γ . The contours show the values of the thermally averaged cross-sections $a_{\gamma\gamma}$ (a) and $a_{\gamma Z}$ (b) in cm^3s^{-1} for $y_{12} = -y$. Again $y_{12} = 0$ results in an almost identical plot.

These bounds depend strongly on the DM halo profile¹¹ (and the region of interest) that one follows. Thus, we study the profile which gives the strongest bound. This comes from the $R3$ region which is optimized for the Navarro-Frenk-White NFWc($\gamma = 1.3$) profile [76] (the relevant discussion on these regions of interest is found in [59]). So, the annihilation cross-section for $\chi_1^0\chi_1^0 \rightarrow \gamma\gamma$ for this region of interest is bounded to be smaller than $\sim 10^{-28} \text{ cm}^3\text{s}^{-1}$ for photon energy ($E_\gamma = m_{\chi_1^0}$) at 200 GeV up to $\sim 3.5 \times 10^{-28}$ for $E_\gamma \sim 450$ GeV (and if we extrapolate up to $\sim 5 \times 10^{-28}$ for $E_\gamma \sim 500$ GeV). For the process $\chi_1^0\chi_1^0 \rightarrow \gamma Z$, we need to rescale this bound by a factor of two, since there is one photon in the final state instead of two. This process results to different value of $E_\gamma = m_{\chi_1^0} (1 - m_Z^2/4m_{\chi_1^0}^2)$.

Fig. 19 illustrates that the annihilation to γZ (and less to $\gamma\gamma$), violates the Fermi-LAT bound, mainly for larger values of E_γ . Thus, the values of d_W and d_γ are constrained so that C_γ is even smaller than the cosmologically acceptable values. It is evident from Fig. 20a, that in order this model to deceive the current monochromatic gamma ray bounds from GC, we should limit the dipole couplings so they satisfy the relation $|d_W s_W - c_W d_\gamma| \lesssim 0.05$ ($\Lambda = 1 \text{ TeV}$) for $M_D = 200 \text{ GeV}$ up to $|d_W s_W - c_W d_\gamma| \lesssim 0.15$ for $M_D = 500 \text{ GeV}$. Therefore, one can delineate accordingly the parameter space on the $d_W - d_\gamma$ plane, that evades all bounds and yields the correct relic density, which is shown in Fig. 20b. It should be noted, that the other parameters remain unchanged as in the previous section, since they do not affect WIMP pair annihilation rates to two photons or to a photon and a Z boson. Other values of y_{12} result to almost identical regions to these in Fig. 20.

Concluding this paragraph, we note that the Fermi-LAT data set upper bounds to the

¹¹The bounds have up to a factor of 15 difference for different profiles and regions.

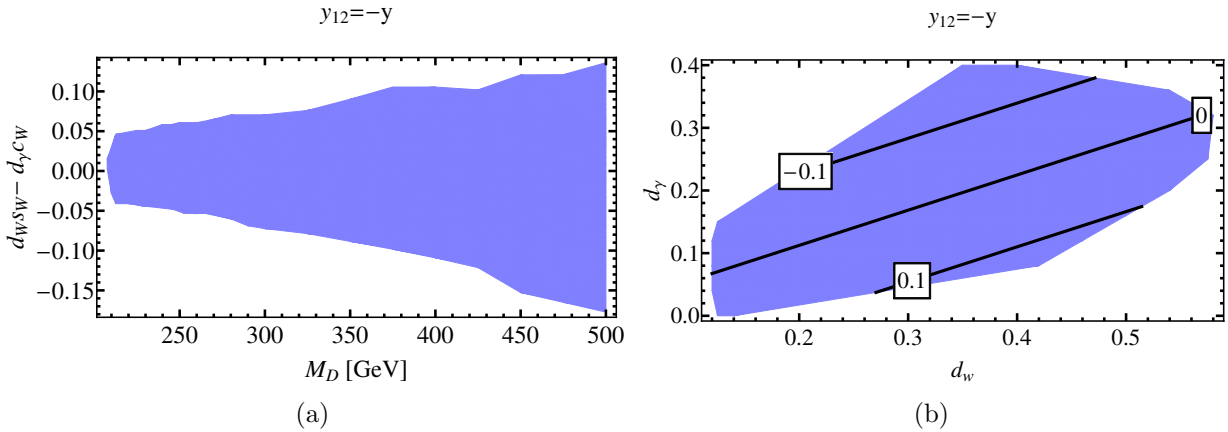


Figure 20: Allowed regions on a) $M_D - C_\gamma$ plane and b) $d_W - d_\gamma$ plane for $y_{12} = -y$, consistent with “Earth” constraints, the observed relic abundance and the bounds from gamma-ray monochromatic spectrum, discussed sections 4, 5.3 and 5.4.2, respectively, in the text. Almost identical regions are allowed for $y_{12} = 0$. The contour lines in (b) show the value of the $\chi_1^0 \chi_2^0$ -photon coupling C_γ .

annihilation cross-section of two WIMPs into one or two photons, relating strongly the two dipole couplings, resulting to positive values for d_γ . Therefore, the two neutral particles of the model have an almost zero coupling to photon ($C_\gamma \approx 0$), while the other parameters are intact.

It is worth pointing out that there is a non-relativistic non-perturbative effect, known as “Sommerfeld enhancement” [77], that can boost the annihilation cross-section, sometimes even, by orders of magnitude. For the bi-doublet case here, it has been calculated in the literature and the results are shown in refs. [78–80]. As it turns out, for the masses we are considering here, this effect is non-important. It becomes only sizeable for WIMP, “higgsino-like” masses greater than about 1 TeV or so.

5.5 Neutrino flux from the Sun

Another interesting indirect signal could come from solar neutrino flux. The cross-section for neutrino production from WIMP annihilations in the Sun, can be decomposed to the spin-dependent and spin-independent WIMP-nucleon cross-sections. Therefore, such experiments compete with direct detection ones. Recent results from IceCube [63], show that the spin-independent cross-section bound is relaxed as compared to the one obtained from direct detection experiments [46]. On the other hand, the latest spin-dependent cross-section bound from solar neutrino flux [62], is much stronger than the one derived from LUX [81] for $m_{\chi_1^0} \gtrsim 200$ GeV. In our study, the spin-independent bound from IceCube is evaded, since the constraints from LUX have been introduced from the beginning of this analysis. In addition, due to the c.c. symmetry, the spin-dependent cross-section vanishes, since $\chi_1^{0\dagger} \bar{\sigma}^\mu \chi_1^0 Z_\mu$ is odd under the transformation introduced in section 2. Thus, these bounds, leave the allowed parameter space unaffected.

6 LHC searches

Having found that there is a viable area in the parameter space, which produces the observed DM relic abundance of the universe while avoiding all the other experimental and observational constraints, we move on to find out whether this theory can provide us with observational effects at the LHC. First, we calculate the cross-sections for some channels at $\sqrt{\hat{s}} = 8$ TeV and compare them to the current bounds from LHC (Run I) and then we do the same at RunII with $\sqrt{\hat{s}} = 13$ TeV.

In this section we are looking at the mono- Z channel for which the experimental analysis is performed by ATLAS [82], the mono- W channel where we use the results from ATLAS [83] (a weaker bound is obtained from the analysis of CMS [84]), the hadronically decaying W/Z boson channel searched for by ATLAS [85]. DM interacting with vector bosons can be probed by dijet searches through vector boson fusion as discussed in refs. [86, 87]. The analysis has been performed by ATLAS [88]¹² (which gives a somewhat stronger bound than CMS [89]). Furthermore, there are mono-jet searches from CMS [90]. Finally, there is also the mono-photon channel searches [85, 91], but in our case it is not very important due to the Fermi-LAT bound discussed previously in section 5.4.2.

We note that, for these processes, an extensive study has been performed in ref. [9] with singlet Dirac DM particle and for operators with dimension $d = 7$. However, in the analysis we perform here there are differences: *a)* The set of operators is different, since we consider Yukawa, dipole and renormalizable operators. These operators produce mass splittings between the Dark-sector fermions. In addition to this, the interactions with the gauge bosons come from both 3- and 4-point terms in the Lagrangian with different Lorentz structure than the $d = 7$ ones. *b)* The parameter space in which we calculate the cross-sections for these processes, respects other experimental and observational constraints. In addition, for the dijet channel and at $\sqrt{\hat{s}} = 13$ TeV, another dedicated study has been performed in ref. [92]. Again our case is different because of the inclusion of $d = 4$ and 5 operators in the calculations of the LHC cross-sections, while at the same time the parameter space is also constrained by all the other bounds discussed in sections 4 and 5.

6.1 LHC constraints at 8 TeV

In this paragraph we calculate the cross-sections for the relevant channels at 8 TeV and compare them to the current bounds from LHC. The bounds we use throughout this analysis are:

- *Mono-Z*: $pp \rightarrow \chi_1^0 \chi_1^0 + (Z \rightarrow l^+ l^-)$, $l = e, \mu$, with cross-section $\lesssim 0.27$ fb [82].
- *Mono-W*: $pp \rightarrow \chi_1^0 \chi_1^0 + (W \rightarrow \mu \nu_\mu)$, with cross-section $\lesssim 0.54$ fb [83].
- *Hadronically decaying Z/W*: $pp \rightarrow \chi_1^0 \chi_1^0 + (W/Z \rightarrow \text{hadrons})$, with $\sigma_{\cancel{E}_T + \text{hadrons}} \lesssim 2.2$ fb [85].
- *Dijet*: $pp \rightarrow \chi_1^0 \chi_1^0 + 2 \text{ jets}$, with $\lesssim 4.8$ fb [88].
- *Mono-jet*: $pp \rightarrow \chi_1^0 (\chi_2^0 \rightarrow \chi_1^0 + \nu \bar{\nu}) + \text{jet}$ with $\sigma_{\cancel{E}_T + \text{jet}} \lesssim 6.1$ fb [90].

¹²The fermions considered here, do not contribute to the invisible decays of the Higgs boson, but bounds from ref. [88] still apply for a dijet + \cancel{E}_T final state.

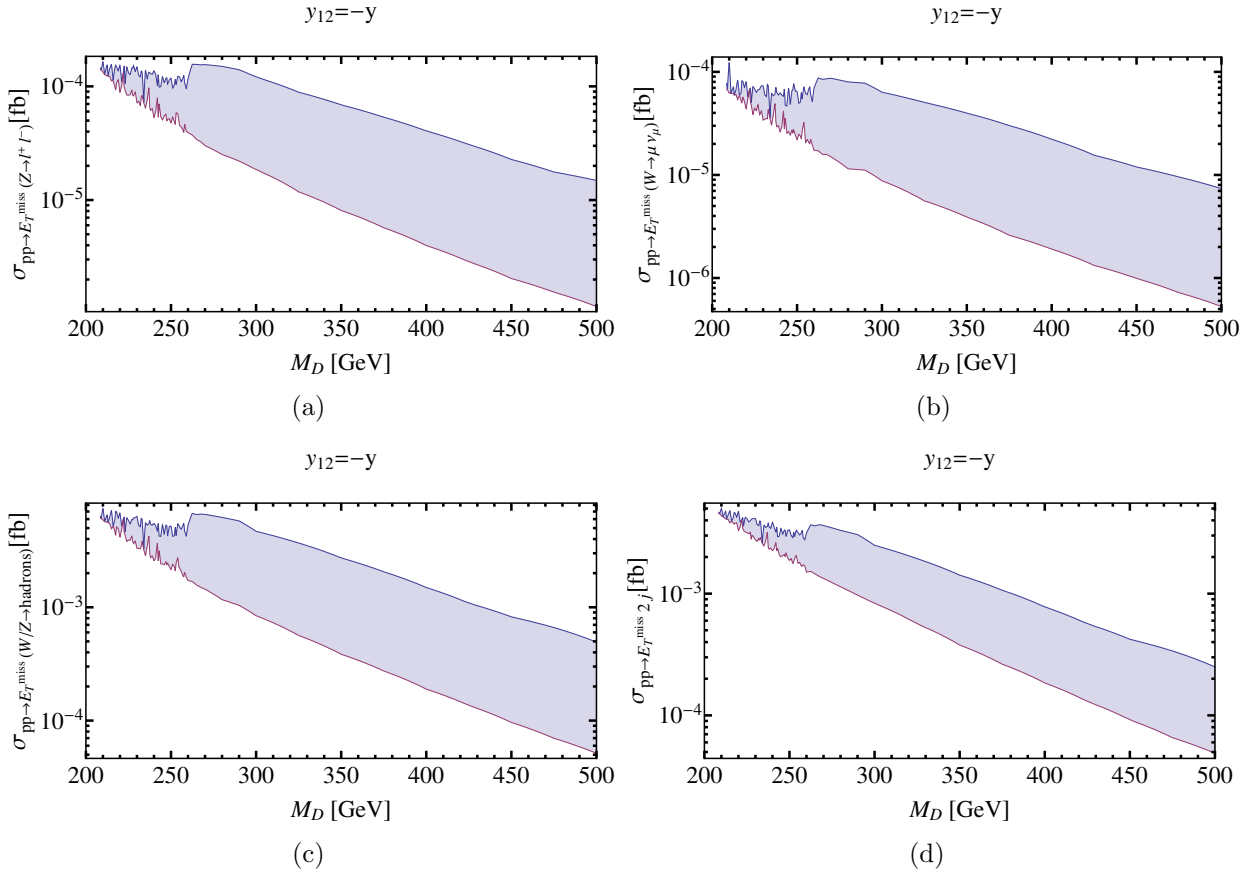


Figure 21: *The cross-sections for the (a) mono-Z, (b) mono-W, (c) hadronically decaying Z/W and (d) the dijet processes at $\sqrt{s} = 8$ TeV versus the doublet-mass parameter M_D , while all the other parameters run freely and for $y_{12} = -y$. The other case with $y_{12} = 0$ gives almost identical results. The “spikes” appeared is a result of varying a random selection of parameters.*

The cross-sections for the first four channels in the allowed parameter space are shown in Fig. 21. It is apparent that the current bounds of LHC for these processes cannot put any further restrictions to the allowed parameter space. On top of that, as M_D becomes larger, the cross-sections decrease. There are two reasons for this. First, as M_D increases, the masses increase, and, second, the dipole moments d_W and d_γ relevant for the observed relic abundance, move to smaller values as M_D becomes larger (see Fig. 14), which reduces the interaction strength of the WIMP to the gauge bosons.

We should point out that we only calculate the cross-sections of the hard processes (before showering, jet reconstruction, etc.).¹³ This means that in general, the actual cross-sections should be smaller than the ones we present here, since the cuts we are able to use for the hard processes are weaker than the cuts used in the experimental analyses.

¹³For the calculation we use the program CalcHEP v.3.6 of ref. [93].

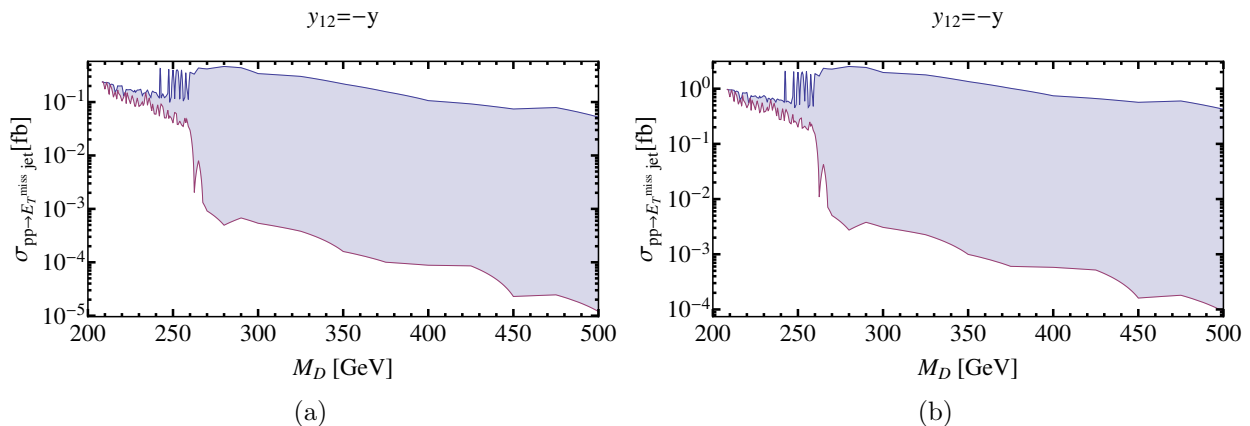


Figure 22: As in Fig. 21 for the mono-jet channel with (a) $\sqrt{\hat{s}} = 8$ TeV and (b) $\sqrt{\hat{s}} = 13$ TeV.

The cross-section for the mono-jet channel¹⁴ is shown in Fig. 22a. Again, as it can be seen, the cross-section is significantly smaller than the current bound from LHC. Additionally, similar to the other channels discussed here, as M_D increases, the cross-section tends to decrease. But, since this cross-section depends strongly on both the dipole moments, d_γ and d_W , and the Yukawa coupling y (through the branching ratio of $\chi_2^0 \rightarrow \chi_1^0 + \nu\bar{\nu}$), the shaded area is larger than the areas in Fig. 21, because the available values of y do not depend strongly on M_D (see Fig. 15). Also, it is apparent from Figs. 21 and 22(a), that for future DM searches at the LHC (for the model we study here), the mono-jet channel seems to be the most promising, since it could result to the largest number of events compared to other channels discussed here.

6.2 Mono-jet searches at 13 TeV

For LHC (RunII) with $\sqrt{\hat{s}} = 13$ TeV, the mono-jet channel provides the biggest number of events when compared to other channels. From Fig. 22b, we observe that the production of a jet accompanied with missing E_T , can reach cross sections up to ~ 2.5 fb for both cases $y_{12} = 0$ and $y_{12} = -y$ and for $M_D \approx 300$ GeV. This means that the number of events that can, in principle, be observed¹⁵ is around 250 (750) for LHC expected luminosity reach of 100 (300) fb^{-1} .

Before closing this section, we should remark issues about the validity of our calculations at such high center-of-mass energy. The validity of calculations for such theories at the LHC depends on the cut off energy and the couplings. The energy for which the calculation of an observable becomes invalid is $\sim \Lambda/C$,¹⁶ where C is the Wilson coefficient for the relevant operator. In our case, and for the mono-jet searches, the relevant $d = 5$ term (a Feynman diagram is shown in Fig.23) is $C \chi_1^0 \sigma_{\mu\nu} \chi_2^0 F_Z^{\mu\nu}$ with $C \sim c_W d_W + s_W d_\gamma$. Thus, if the pair of $\chi_1^0 \chi_2^0$ particles are produced with energy larger than $\sim \Lambda(c_W d_W + s_W d_\gamma)^{-1}$, the calculation is considered to be inaccurate. In order to understand this, a numerical example is given in

¹⁴We approximate this cross-section by $\sigma_{pp \rightarrow \chi_1^0 \chi_2^0} \times \sum_{i=e,\mu,\tau} BR_{\chi_2^0 \rightarrow \chi_1^0 \nu_i \bar{\nu}_i}$.

¹⁵Very recently, a mono-jet+photon search has been proposed in ref. [94]. Emphasised for higgsinos, this final state can often be as competitive as the monojet channel.

¹⁶This holds under the assumption that the couplings of the *UV complete* model are ~ 1 .

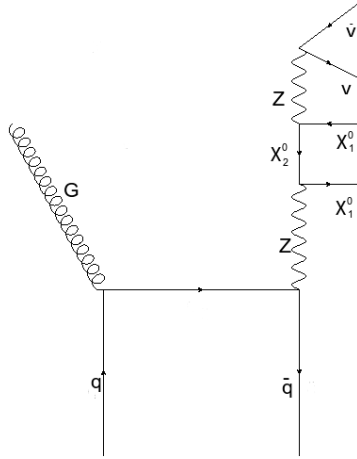


Figure 23: A Feynman diagram for the mono-jet process. The time “runs” upwards.

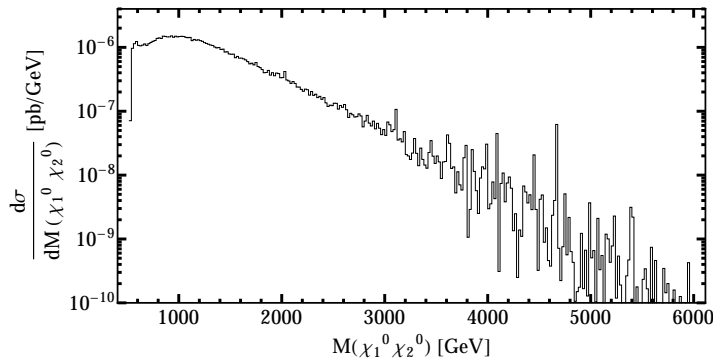


Figure 24: The dependence of the mono-jet differential cross-section, $d\sigma/dM(\chi_1^0\chi_2^0)$, on the invariant mass for the pair of the neutral fermions, for $\sqrt{s} = 13$ TeV, $M_D = 250$ GeV, $d_W = 0.45$ and $d_\gamma = 0.25$.

Fig. 24, where the dependence of the differential cross-section on the invariant mass of the dark sector particles (which measures the energy that would be transferred by the integrated out particle) is shown for $M_D = 250$ GeV, $d_W = 0.45$ and $d_\gamma = 0.25$. We observe that above ~ 2 TeV, the mono-jet differential cross-section falls rapidly, and, the main contribution to the inclusive cross-section, around 85% for this particular example, arises for invariant masses with $M(\chi_1^0\chi_2^0) \lesssim 2$ TeV. In addition, since $C \approx 0.5$ and $\Lambda = 1$ TeV, the energy scale where this calculation is inaccurate is $\frac{\Lambda}{C} \sim 2$ TeV, and therefore this calculation is, in principle, reliable.

Furthermore, the limit discussed above could be different, since the expansion of the *UV complete* model is generally written in powers of $\frac{\lambda}{M}$, where λ is a generic coupling (or a function of couplings) of this model and M is the mass of the particle which is integrated out. The convergence of this expansion depends on the value of $\frac{\lambda}{M}$ which is, in principle, different from $\frac{C}{\Lambda}$. An extensive discussion on the limitations of effective theories at the LHC can be found in refs. [95, 96]. Finally, as shown in ref. [97], there are cases where the decay width of the particle that is integrated out vastly affects the cross-section. There are also UV independent bounds coming from unitarity, discussed in refs. [98, 99]. A detailed study

of these effects is beyond the scope of this paper.

7 Conclusions

We have introduced in the SM particle spectrum a fermionic bi-doublet: a pair of Weyl fermion $SU(2)_L$ -doublets, \mathbf{D}_1 and \mathbf{D}_2 , with opposite hypercharges. In addition, we assume a discrete Z_2 -symmetry that distinguishes \mathbf{D}_1 and \mathbf{D}_2 from the SM fields. This anomaly free set of fermions, together with the Z_2 -symmetry are quite common features in non-supersymmetric $SO(10)$ GUT constructions for light dark matter. Light $SU(2)_L$ doublets, whose components are parts of the WIMP have been also considered countless of times in “UV-complete” non-supersymmetric or supersymmetric models (*i.e.*, higgsino dark matter). Our work is related to these UV models when all other particles but the doublets have been integrated out in their low energy spectrum.

At the renormalizable level the mass spectrum consists of a electromagnetically neutral, and a charged Dirac, fermions. Under the presence of $d = 5$ operators, the neutral Dirac fermion is split into two Majorana states, the WIMP, χ_1^0 , and its excited state, χ_2^0 . Moreover, the $d = 5$ operators include magnetic and electric dipole transitions which are, in principle, generated by a UV-complete theory, possibly at the TeV scale. We ask here the question whether the dark matter particle χ_1^0 , with mass ($m_{\chi_1^0}$), *around the EW scale*, is compatible to various collider, astrophysical and cosmological data.

In order to reduce fine tuning and extensive scans of the parameter space, in section 3.1 we adopted four scenarios, a,b,c and d, based on well motivated symmetry limits of the theory such as a charge conjugation or a custodial symmetry that act on \mathbf{D} 's and Higgs field H . These low energy symmetries simplify enough the analytical expressions of the interactions and possibly help to construct UV-completions of the model. After collecting all relevant $d = 5$, and $d = 6$ (though the latter not used in the analysis), operators in the Appendix A, we went on to investigate their implications into collider and astrophysical processes.

In section 4, we performed a constraint analysis based (*i*) on scattering WIMP-nucleus recoiling experiments, such as LUX, (*ii*) on LEP searches for new fermions, as well as (*iii*) on LHC searches for the decay $h \rightarrow \gamma\gamma$. Bounds on the model parameters (2.17) are collected in Fig. 4. Only in cases (b) and (c) there is still enough freedom to carry on. In the same section, we also studied contributions from the new fermion interactions into oblique electroweak S, T and U parameters. Only the S parameter is affected, and, as a consequence, only case (a) is further constrained.

Focused on the more interesting cases (b) and (c), in section 5 we calculated the relic density Ωh^2 for χ_1^0 . In the presence of $d = 5$ dipole operators there are destructive interference effects in the (dominant) amplitudes for WIMP annihilations (or co-annihilations) into SM vector bosons. The minima in the cross sections correspond to certain, usually non-zero, values for the coefficients of the dipole operators d_W and d_γ [see eqs. (5.13a) and (5.13b)]. Nearby these minima the relic density is found to be consistent with observation [eq. (1.1)] for $m_{\chi_1^0} \gtrsim 200$ GeV. Although continuous gamma ray spectrum constraints are harmless, constraints from monochromatic gamma ray spectrum are serious for the photon dipole coupling as it is shown in Figs. 19 and 20. The coefficient d_W has to be more than 10% a value which is non-negligible for UV models with Dark matter at the EW scale. d_γ on the other hand can be tuned to zero without a problem.

Apart from possible aesthetics, the main reason in insisting for EW dark matter mass, $m_{\chi_1^0} \approx M_Z$, has to do with enhancing the possibility of observing the dark sector at the LHC (or, in any case, to be as close as visible in the RunII phase). In section 6 we estimated the cross section for producing χ_1^0 at LHC with center of mass energy $\sqrt{\hat{s}} = 8, 13$ TeV and in association with a jet (monojet) or 2 jets or a W or a Z . We found that the monojet process is the most promising with a few hundred of events at $\sqrt{\hat{s}} = 13$ TeV and with $m_{\chi_1^0} \simeq 200 - 350$ GeV (see Fig. 22).

Searching for dark matter and/or related particles at LHC consists in a major effort from physicists in high energy physics and astrophysics. An effective field theory for an electroweak dark matter described in this article may guide us closing that goal.

Acknowledgements

AD would like to thank CERN Theory Division for the kind hospitality and Apostolos Pilaftsis for useful discussions. DK would like to thank Alexander Pukhov for his helpful advices in setting up CalcHEP.

This research has been co-financed by the European Union (European Social Fund - ESF) and Greek national funds through the Operational Program “Education and Lifelong Learning” of the National Strategic Reference Framework (NSRF) - Research Funding Programs: THALIS and ARISTEIA - Investing in the society of knowledge through the European Social Fund.

Appendix A Non-renormalizable operators

Apart from the mass term in eq. (2.1), and the renormalizable couplings to gauge bosons discussed in section 3, the “ D ”-doublets couple to the bosons of the theory through non-renormalizable $d = 5, 6$ interactions. Gauge numbers, denoted as $(SU(3)_C, SU(2)_L)_{U(1)_X}$, for the particles here are: for quarks $\mathbf{Q} \sim (\mathbf{3}^c, \mathbf{2})_{\frac{1}{3}}$, $\bar{\mathbf{u}} \sim (\mathbf{3}^c, \mathbf{1})_{-\frac{4}{3}}$, $\bar{\mathbf{d}} \sim (\mathbf{3}^c, \mathbf{1})_{+\frac{2}{3}}$, for leptons: $\mathbf{L} \sim (\mathbf{1}^c, \mathbf{2})_{-1}$, $\bar{\mathbf{e}} \sim (\mathbf{1}^c, \mathbf{1})_{+2}$, for the Higgs doublet: $\mathbf{H} \sim (\mathbf{1}^c, \mathbf{2})_{+1}$ and finally for the new bi-doublets: $\mathbf{D}_1 \sim (\mathbf{1}^c, \mathbf{2})_{-1}$ and $\mathbf{D}_2 \sim (\mathbf{1}^c, \mathbf{2})_{+1}$. Schematically, the possible interactions are: $ffHH$, $ff\mathcal{D}H$, $ff\mathcal{D}\mathcal{D}$, where \mathcal{D} is the covariant derivative acting in both Weyl fermions f or to the Higgs fields. We arrange all Weyl fermions f to be left-handed.

We list below all relevant possible independent $d = 5$ and $d = 6$ operators. An analogous list has been constructed in ref. [100] but for the fermionic *singlet* extension of the SM. The complete set of $d = 5, 6$ Standard Model operators can be read from ref. [101].

Appendix A.1 $d = 5$ non-renormalizable operators

- $ffHH$: The $d = 5$ operators alter the DM mass spectrum and the Higgs-boson interactions with the dark sector obtained for $f = D_1, D_2$, when integrating out heavy particles. Examples of possible simplified models that result into these operators, are obtained by integrating out fermion neutral singlets (S_0) and triplets (T), fermion charged singlets (S^\pm) and triplets (T^\pm), or scalar singlets, (Φ_{S_0}, Φ_{S^\pm}) and triplets, (Φ_{T^0}, Φ_{T^\pm}). In fully $SU(2)_L$ -invariant form we have

$$\begin{aligned}
- \mathcal{L}_{\text{dim}=5} \supset & + \frac{\lambda_1^2}{2M_{S_0}} (\epsilon^{ab} H_a D_{1b}) (\epsilon^{cd} H_c D_{1d}) + \frac{\lambda_2^2}{2M_{S_0}} (H^{\dagger a} D_{2a}) (H^{\dagger b} D_{2b}) \\
& + \frac{\lambda_{12}}{M_{S_0}} (\epsilon^{ab} H_a D_{1b}) (H^{\dagger c} D_{2c}) + \frac{\lambda'_{12}}{M_{S^\pm}} (\epsilon^{ab} H_a D_{2b}) (H^{\dagger c} D_{1c}) \\
& + \frac{Y_1^2}{2M_T} [\epsilon^{ab} H_a (\tau^A)_b^c D_{1c}] [\epsilon^{fg} H_f (\tau^A)_g^h D_{1h}] + \frac{Y_2^2}{2M_T} [H^{\dagger a} (\tau^A)_a^b D_{2b}] [H^{\dagger c} (\tau^A)_c^d D_{2d}] \\
& + \frac{Y_{12}}{M_T} [H^{\dagger a} (\tau^A)_a^b D_{2b}] [\epsilon^{cd} H_c (\tau^A)_d^f D_{1f}] + \frac{Y'_{12}}{M_{T^\pm}} [H^{\dagger a} (\tau^A)_a^b D_{1b}] [\epsilon^{cd} H_c (\tau^A)_d^f D_{2f}] \\
& + \frac{\xi_{12}}{M_{\Phi_0}} (\epsilon^{ab} D_{1a} D_{2b}) (H^{\dagger c} H_c) \\
& + \frac{k_1^2}{2M_{\Phi_\mp}} [\epsilon^{ab} D_{1a} (\tau^A)_b^c D_{1c}] [\epsilon^{fg} H_f (\tau^A)_g^h H_h] + \frac{k_2^2}{2M_{\Phi_\mp}} [\epsilon^{ab} D_{2a} (\tau^A)_b^c D_{2c}] [H^{\dagger d} (\tau^A)_d^f \epsilon_{fg} H^{\dagger g}] \\
& + \frac{k_{12}}{M_{\Phi_{T_0}}} [\epsilon^{ab} D_{1a} (\tau^A)_b^c D_{2c}] [H^{\dagger d} (\tau^A)_d^g H_g] + \frac{k'_{12}}{M_{\Phi_{T_0}}} [\epsilon^{ab} D_{2a} (\tau^A)_b^c D_{1c}] [H^{\dagger d} (\tau^A)_d^g H_g] \\
& + \text{H.c.} , \tag{A.1}
\end{aligned}$$

where the meaning of various mass scales is rather obvious e.g., those suppressed by M_{S_0}, M_{S^\pm} and M_{T, T^\pm} are derived from integrating out heavy fermionic neutral and/or charged singlets and triplets S_0, S^\pm and, T, T^\pm respectively, and so on.

However, not all operators in eq. (A.1) are independent; in fact most of them are not. Using a standard identity for Pauli matrices, $(\tau^A)_{ab}(\tau^A)_{cd} = 2(\delta_{ad}\delta_{bc} - \frac{1}{2}\delta_{ab}\delta_{cd})$, one can arrive at the most general form of (A.1) written as

$$\begin{aligned} -\mathcal{L}_{\text{dim}=5} \supset & + \frac{y_1}{2\Lambda} (\epsilon^{ab} H_a D_{1b}) (\epsilon^{cd} H_c D_{1d}) + \frac{y_2}{2\Lambda} (H^{\dagger a} D_{2a}) (H^{\dagger b} D_{2b}) \\ & + \frac{y_{12}}{\Lambda} (\epsilon^{ab} H_a D_{1b}) (H^{\dagger c} D_{2c}) + \frac{\xi_{12}}{\Lambda} (\epsilon^{ab} D_{1a} D_{2b}) (H^{\dagger c} H_c) + \text{H.c.} \end{aligned} \quad (\text{A.2})$$

where we use a common mass scale Λ at which heavy particles are integrated out and the complex valued Yukawa couplings $y_1, y_2, y_{12}, \xi_{12}$. We should also remark that the last operator in (A.2) is somewhat trivial and it can appear in any powers of the Higgs polynomial. At EW vacuum it adds a common mass to D_1 and D_2 as in eq. (2.1) does. All operators in (A.2) give masses to neutral components of the WIMPs except from the last one that gives mass also to the charged components.

Furthermore, in this class belongs the famous Weinberg operator for neutrino masses, with $f = L$ being the SM lepton doublet

$$\frac{y_\nu}{2\Lambda} (\epsilon^{ab} H_a L_b) (\epsilon^{cd} H_c L_d) + \text{H.c.} \quad (\text{A.3})$$

The origin of this operator is not necessarily related to the DM sector. Note that the first three terms in eq. (A.2), can also be obtained by integrating out heavy right-handed neutrino states, $\bar{\nu} \sim (\mathbf{1}^c, \mathbf{1})_{\mathbf{0}}$, from renormalizable Yukawa couplings, $H^{\dagger} D_2 \bar{\nu} + H D_1 \bar{\nu} + \text{H.c.}$ as in the see-saw model for neutrino masses.

Of course there are additional terms, *e.g.*, $LD_2 HH$, but these in general, break the Z_2 -discrete (or lepton number) symmetry that keeps the DM particle stable. Interestingly enough, these terms are connecting the DM particle to neutrinos, see for instance [102]. These independent operators are

$$\begin{aligned} & \frac{\eta_1}{2\Lambda} (\epsilon^{ab} H_a D_{1b}) (\epsilon^{cd} H_c L_d) + \frac{\eta_{12}}{\Lambda} (\epsilon^{ab} H_a L_b) (H^{\dagger c} D_{2c}) \\ & + \frac{\zeta_{12}}{\Lambda} (\epsilon^{ab} L_a D_{2b}) (H^{\dagger c} H_c) + \text{H.c.} \end{aligned} \quad (\text{A.4})$$

- $ff\mathcal{D}H$: In this case the fermion bilinear must be a weak doublet with hypercharge -1 . The only such combination, $D_2^{\dagger} \bar{\sigma}^{\mu} \bar{e} \mathcal{D}_{\mu} H^{\dagger} + \text{H.c.}$, is not invariant under the Z_2 -symmetry.
- $ff\mathcal{D}\mathcal{D}$: Under Z_2 -symmetry there are three possibilities : $D_1 \mathcal{D} \mathcal{D} D_2$, $\mathcal{D} \mathcal{D} D_1 D_2$ and $\mathcal{D} D_1 \mathcal{D} D_2$. After some algebra, and taking the equations of motion into account we find that these lead to dipole operators of the form

$$\begin{aligned} & \frac{d_\gamma}{\Lambda} \epsilon^{ab} D_{1a} \sigma^{\mu\nu} D_{2b} B_{\mu\nu} + \frac{d_W}{\Lambda} \epsilon^{ab} D_{1a} \sigma^{\mu\nu} (\tau^A)_b^c D_{2c} W_{\mu\nu}^A + \\ & \frac{i e_\gamma}{\Lambda} \epsilon^{ab} D_{1a} \sigma^{\mu\nu} D_{2b} \tilde{B}_{\mu\nu} + \frac{i e_W}{\Lambda} \epsilon^{ab} D_{1a} \sigma^{\mu\nu} (\tau^A)_b^c D_{2c} \tilde{W}_{\mu\nu}^A + \text{H.c.}, \end{aligned} \quad (\text{A.5})$$

where $B_{\mu\nu}$ and $W_{\mu\nu}^A$ are the $U(1)$ and $SU(2)_L$, field strength tensors, respectively, and $\tilde{B}_{\mu\nu} \equiv \epsilon_{\mu\nu}^{\rho\sigma} B_{\rho\sigma}$. These operators are electric and magnetic dipole moments for the DM particle. They arise directly at $d = 5$ level, whereas quark and/or lepton magnetic moments arise at $d = 6$ level.

We have not found other than the above $d = 5$ independent operators.

Appendix A.2 $d = 6$ non-renormalizable operators

Focusing only in interactions between $f = D_1$ or D_2 and the Higgs field¹⁷ there are four Lorentz and gauge invariant categories: ffH^3 , $ff\mathcal{D}H^2$, $ff\mathcal{D}^2H$, $ff\mathcal{D}^3$, and of course $ffff$.

- ffH^3 : There are no such operators which preserve the Z_2 -symmetry, or, as a matter of fact, the charge conjugation or custodial symmetry or lepton number, e.g. there is $(H^\dagger D_1 \bar{e})(H^\dagger H)$ and the one with triplets.
- $ff\mathcal{D}H^2$: There are quite a few invariant operators of this kind. The independent ones are

$$\begin{aligned}
- \mathcal{L}_{\text{dim}=6} \supset & \left(\frac{a_1}{\Lambda^2} D_1^{\dagger a} \bar{\sigma}^\mu D_{1a} + \frac{a_2}{\Lambda^2} D_2^{\dagger a} \bar{\sigma}^\mu D_{2a} \right) \left(i H^{\dagger b} (\overleftrightarrow{\mathcal{D}}_\mu)_b^c H_c \right) \\
& + \left(\frac{a'_1}{\Lambda^2} D_1^{\dagger a} (\tau^A)_a^b \bar{\sigma}^\mu D_{1b} + \frac{a'_2}{\Lambda^2} D_2^{\dagger a} (\tau^A)_a^b \bar{\sigma}^\mu D_{2b} \right) \left(i H^{\dagger c} (\overleftrightarrow{\mathcal{D}}_\mu)_c^d H_d \right) \\
& + \frac{b_1}{\Lambda^2} (D_2^{\dagger a} \bar{\sigma}^\mu D_{1a}) [\epsilon^{bc} H_b (\overleftrightarrow{\mathcal{D}}_\mu)_c^d H_d] + \frac{b_2}{\Lambda^2} (D_1^{\dagger a} \bar{\sigma}^\mu D_{2a}) (\epsilon_{bc} H^{\dagger b} (\overleftrightarrow{\mathcal{D}}_\mu)_c^d H^{\dagger d})
\end{aligned} \tag{A.6}$$

where $H^\dagger \overleftrightarrow{\mathcal{D}}_\mu H \equiv H^\dagger \overrightarrow{\mathcal{D}}_\mu H - H^\dagger \overleftarrow{\mathcal{D}}_\mu H$ and $H^\dagger \overleftrightarrow{\mathcal{D}}_\mu^A H \equiv H^\dagger \tau^A \overrightarrow{\mathcal{D}}_\mu H - H^\dagger \overleftarrow{\mathcal{D}}_\mu \tau^A H$, $a_{1,2}$ and $a'_{1,2}$ are real numbers, while $b_2 = b_1^*$. We can obtain new operators after changing $L \leftrightarrow D_1$ but these would violate Z_2 or they would belong to existing SM operators given in ref. [101].

- $ff\mathcal{D}^2H$: Because D_1, D_2 and the H are $SU(2)$ -doublets only Z_2 -breaking terms exist in this category, e.g., $(D_1 \sigma_{\mu\nu} \bar{e}) F^{\mu\nu} H^\dagger$ or when the Higgs receives vev they reduce to $d = 5$ operators already given in (A.5).
- $ff\mathcal{D}^3$: We found no new operators. Lorentz invariance says that they exist only if ff transforms as a vector e.g., $(D_1^\dagger \bar{\sigma}_\mu D_1) (\mathcal{D}_\rho B^{\rho\mu})$. By using equations of motion we get at most the operators of eq. (A.6), or the four fermion operators, $ffff$, given below and/or other like previously violating Z_2 -symmetry. Acting with the covariant derivative to the left (on fermion current) we obtain operators as in eq. (A.5).
- $ffff$: we found the following independent operators:

$$\begin{aligned}
- \mathcal{L}_{\text{dim}=6} \supset & \frac{c_{12}}{\Lambda^2} (\epsilon^{ab} D_{1a} D_{2b}) (\epsilon^{cd} D_{1c} D_{2d}) + \sum_{k,\ell=1}^2 \frac{d_{k\ell}}{\Lambda^2} (D_k^{\dagger a} \bar{\sigma}^\mu D_{ka}) (D_\ell^{\dagger b} \bar{\sigma}_\mu D_{\ell b}) \\
& + \sum_{i,j=1}^3 \sum_{k=1}^2 \frac{1}{\Lambda^2} (D_k^{\dagger a} \bar{\sigma}^\mu D_{ka}) \left[f_{kij}^\ell (\ell_i^\dagger \bar{\sigma}_\mu \ell_j) + f_{kij}^q (q_i^\dagger \bar{\sigma}_\mu q_j) \right] + \\
& + \sum_{i,j=1}^3 \sum_{k=1}^2 \frac{1}{\Lambda^2} (D_k^{\dagger a} \bar{\sigma}^\mu (\tau^A)_a^b D_{kb}) \left[c_{kij}^L (L_i^{\dagger c} \bar{\sigma}_\mu (\tau^A)_c^d L_j d) + c_{kij}^Q (Q_i^{\dagger c} \bar{\sigma}_\mu (\tau^A)_c^d Q_j d) \right] \\
& + \frac{c'_{12}}{\Lambda^2} (D_1^{\dagger a} \bar{\sigma}^\mu (\tau^A)_a^b D_{1b}) (D_2^{\dagger c} \bar{\sigma}^\mu (\tau^A)_c^d D_{2d}) + \text{H.c.},
\end{aligned} \tag{A.7}$$

¹⁷All others are identical to standard dimension-6 operators and can be found in [101].

not counting operators that violate Z_2 . Note that $\ell \equiv L, \bar{e}$ and $q \equiv Q, \bar{u}, \bar{d}$ and i, j indices stand for lepton or quark flavour. Furthermore, there is only one scalar $d = 6$ four-fermion operator, the one containing DM-self interactions proportional to c_{12} . In addition, there are lepton number violating *scalar* operators like:

$$(D_{1a}D_{1b})(L^{\dagger a}L^{\dagger b}) + \epsilon^{ac}\epsilon^{bd}(D_{2a}D_{2b})(L_cL_d) + \epsilon^{ab}\epsilon^{cd}(D_{2a}L_b)(D_{2c}L_d). \quad (\text{A.8})$$

Other four-fermion *scalar* operators between quarks/leptons and DM fields appear first at $d = 7$ level and have the form $D_1D_2(QH\bar{u} + QH^{\dagger}\bar{d} + LH^{\dagger}\bar{e})$. All other operators in eq. (A.7) are vector-like, and, many of them lead to spin-dependent interactions in DM-nuclei collisions.

References

- [1] G. Bertone, D. Hooper, and J. Silk, *Particle dark matter: Evidence, candidates and constraints*, *Phys.Rept.* **405** (2005) 279–390, [[hep-ph/0404175](#)].
- [2] G. B. Gelmini, *TASI 2014 Lectures: The Hunt for Dark Matter*, in *Theoretical Advanced Study Institute in Elementary Particle Physics: Journeys Through the Precision Frontier: Amplitudes for Colliders (TASI 2014) Boulder, Colorado, June 2-27, 2014*, 2015. [arXiv:1502.01320](#).
- [3] M. Lisanti, *Lectures on Dark Matter Physics*, in *Theoretical Advanced Study Institute in Elementary Particle Physics: New Frontiers in Fields and Strings (TASI 2015) Boulder, CO, USA, June 1-26, 2015*, 2016. [arXiv:1603.03797](#).
- [4] A. De Simone and T. Jacques, *Simplified Models vs. Effective Field Theory Approaches in Dark Matter Searches*, [arXiv:1603.08002](#).
- [5] **Planck** Collaboration, P. Ade et al., *Planck 2013 results. XVI. Cosmological parameters*, [arXiv:1303.5076](#).
- [6] **Particle Data Group** Collaboration, K. A. Olive et al., *Review of Particle Physics*, *Chin. Phys.* **C38** (2014) 090001.
- [7] L. Roszkowski, *Light neutralino as dark matter*, *Phys.Lett.* **B262** (1991) 59–67.
- [8] M. Drees, M. M. Nojiri, D. Roy, and Y. Yamada, *Light Higgsino dark matter*, *Phys.Rev.* **D56** (1997) 276–290, [[hep-ph/9701219](#)].
- [9] A. Crivellin, U. Haisch, and A. Hibbs, *LHC constraints on gauge boson couplings to dark matter*, *Phys. Rev.* **D91** (2015) 074028, [[arXiv:1501.00907](#)].
- [10] M. S. Carena, A. Megevand, M. Quiros, and C. E. Wagner, *Electroweak baryogenesis and new TeV fermions*, *Nucl.Phys.* **B716** (2005) 319–351, [[hep-ph/0410352](#)].
- [11] R. Mahbubani and L. Senatore, *The Minimal model for dark matter and unification*, *Phys.Rev.* **D73** (2006) 043510, [[hep-ph/0510064](#)].
- [12] F. D’Eramo, *Dark matter and Higgs boson physics*, *Phys.Rev.* **D76** (2007) 083522, [[arXiv:0705.4493](#)].

- [13] T. Cohen, J. Kearney, A. Pierce, and D. Tucker-Smith, *Singlet-Doublet Dark Matter*, *Phys.Rev.* **D85** (2012) 075003, [[arXiv:1109.2604](#)].
- [14] A. Joglekar, P. Schwaller, and C. E. Wagner, *Dark Matter and Enhanced Higgs to Di-photon Rate from Vector-like Leptons*, *JHEP* **1212** (2012) 064, [[arXiv:1207.4235](#)].
- [15] T. Abe, R. Kitano, and R. Sato, *Discrimination of dark matter models in future experiments*, *Phys. Rev.* **D91** (2015), no. 9 095004, [[arXiv:1411.1335](#)].
- [16] S. Banerjee, S. Matsumoto, K. Mukaida, and Y.-L. S. Tsai, *WIMP Dark Matter in a Well-Tempered Regime: A case study on Singlet-Doublets Fermionic WIMP*, [arXiv:1603.07387](#).
- [17] L. Calibbi, A. Mariotti, and P. Tziveloglou, *Singlet-Doublet Model: Dark matter searches and LHC constraints*, *JHEP* **10** (2015) 116, [[arXiv:1505.03867](#)].
- [18] A. Dedes and D. Karamitros, *Doublet-Triplet Fermionic Dark Matter*, *Phys. Rev.* **D89** (2014), no. 11 115002, [[arXiv:1403.7744](#)].
- [19] A. Freitas, S. Westhoff, and J. Zupan, *Integrating in the Higgs Portal to Fermion Dark Matter*, *JHEP* **09** (2015) 015, [[arXiv:1506.04149](#)].
- [20] N. Arkani-Hamed, K. Blum, R. T. D’Agnolo, and J. Fan, *2:1 for Naturalness at the LHC?*, *JHEP* **1301** (2013) 149, [[arXiv:1207.4482](#)].
- [21] C. Arbelaez, R. Longas, D. Restrepo, and O. Zapata, *Fermion dark matter from $SO(10)$ GUTs*, *Phys. Rev.* **D93** (2016), no. 1 013012, [[arXiv:1509.06313](#)].
- [22] N. Nagata, K. A. Olive, and J. Zheng, *Weakly-Interacting Massive Particles in Non-supersymmetric $SO(10)$ Grand Unified Models*, *JHEP* **10** (2015) 193, [[arXiv:1509.00809](#)].
- [23] S. M. Boucenna, M. B. Krauss, and E. Nardi, *Dark matter from the vector of $SO(10)$* , *Phys. Lett.* **B755** (2016) 168–176, [[arXiv:1511.02524](#)].
- [24] C. Garcia-Cely and J. Heeck, *Phenomenology of left-right symmetric dark matter*, [arXiv:1512.03332](#). [[JCAP1603,021\(2016\)](#)].
- [25] F. D’Eramo and M. Procura, *Connecting Dark Matter UV Complete Models to Direct Detection Rates via Effective Field Theory*, *JHEP* **04** (2015) 054, [[arXiv:1411.3342](#)].
- [26] S. Matsumoto, S. Mukhopadhyay, and Y.-L. S. Tsai, *Effective Theory of WIMP Dark Matter supplemented by Simplified Models: Singlet-like Majorana fermion case*, [arXiv:1604.02230](#).
- [27] Y. Mambrini, K. A. Olive, J. Quevillon, and B. Zaldivar, *Gauge Coupling Unification and Nonequilibrium Thermal Dark Matter*, *Phys. Rev. Lett.* **110** (2013), no. 24 241306, [[arXiv:1302.4438](#)].
- [28] C.-K. Chua and G.-G. Wong, *Study of Majorana Fermionic Dark Matter*, 2015. [arXiv:1512.01991](#).

- [29] M. Cirelli, N. Fornengo, and A. Strumia, *Minimal dark matter*, *Nucl.Phys.* **B753** (2006) 178–194, [[hep-ph/0512090](#)].
- [30] E. Del Nobile, R. Franceschini, D. Pappadopulo, and A. Strumia, *Minimal Matter at the Large Hadron Collider*, *Nucl. Phys.* **B826** (2010) 217–234, [[arXiv:0908.1567](#)].
- [31] Y. G. Kim and K. Y. Lee, *The Minimal model of fermionic dark matter*, *Phys.Rev.* **D75** (2007) 115012, [[hep-ph/0611069](#)].
- [32] N. Nagata and S. Shirai, *Higgsino Dark Matter in High-Scale Supersymmetry*, *JHEP* **01** (2015) 029, [[arXiv:1410.4549](#)].
- [33] S. Chang, N. Weiner, and I. Yavin, *Magnetic Inelastic Dark Matter*, *Phys. Rev.* **D82** (2010) 125011, [[arXiv:1007.4200](#)].
- [34] N. Weiner and I. Yavin, *How Dark Are Majorana WIMPs? Signals from MiDM and Rayleigh Dark Matter*, *Phys. Rev.* **D86** (2012) 075021, [[arXiv:1206.2910](#)].
- [35] N. Weiner and I. Yavin, *UV completions of magnetic inelastic and Rayleigh dark matter for the Fermi Line(s)*, *Phys. Rev.* **D87** (2013), no. 2 023523, [[arXiv:1209.1093](#)].
- [36] H. K. Dreiner, H. E. Haber, and S. P. Martin, *Two-component spinor techniques and Feynman rules for quantum field theory and supersymmetry*, *Phys.Rept.* **494** (2010) 1–196, [[arXiv:0812.1594](#)].
- [37] P. Sikivie, L. Susskind, M. B. Voloshin, and V. I. Zakharov, *Isospin Breaking in Technicolor Models*, *Nucl.Phys.* **B173** (1980) 189.
- [38] T. W. B. Kibble, *Symmetry breaking in nonAbelian gauge theories*, *Phys. Rev.* **155** (1967) 1554–1561.
- [39] T. W. B. Kibble, G. Lazarides, and Q. Shafi, *Strings in $SO(10)$* , *Phys. Lett.* **B113** (1982) 237–239.
- [40] M. Frigerio and T. Hambye, *Dark matter stability and unification without supersymmetry*, *Phys. Rev.* **D81** (2010) 075002, [[arXiv:0912.1545](#)].
- [41] **LEP2 SUSY Working Group** Collaboration, *Combined lep chargino results, up to 208 gev for low dm (2001)*, . http://lepsusy.web.cern.ch/lepsusy/www/inoslowdmsummer02/charginolowdm_pub.html.
- [42] **L3** Collaboration, P. Achard et al., *Search for heavy neutral and charged leptons in e^+e^- annihilation at LEP*, *Phys. Lett.* **B517** (2001) 75–85, [[hep-ex/0107015](#)].
- [43] **DELPHI** Collaboration, J. Abdallah et al., *Searches for supersymmetric particles in e^+e^- collisions up to 208-GeV and interpretation of the results within the MSSM*, *Eur. Phys. J.* **C31** (2003) 421–479, [[hep-ex/0311019](#)].
- [44] J. Hisano, D. Kobayashi, N. Mori, and E. Senaha, *Effective Interaction of Electroweak-Interacting Dark Matter with Higgs Boson and Its Phenomenology*, *Phys. Lett.* **B742** (2015) 80–85, [[arXiv:1410.3569](#)].

- [45] C. Cheung, L. J. Hall, D. Pinner, and J. T. Ruderman, *Prospects and Blind Spots for Neutralino Dark Matter*, *JHEP* **05** (2013) 100, [[arXiv:1211.4873](#)].
- [46] **LUX** Collaboration, D. S. Akerib et al., *Improved WIMP scattering limits from the LUX experiment*, [arXiv:1512.03506](#).
- [47] **LUX** Collaboration, D. S. Akerib et al., *First results from the LUX dark matter experiment at the Sanford Underground Research Facility*, *Phys. Rev. Lett.* **112** (2014) 091303, [[arXiv:1310.8214](#)].
- [48] J. Hisano, K. Ishiwata, and N. Nagata, *QCD Effects on Direct Detection of Wino Dark Matter*, *JHEP* **06** (2015) 097, [[arXiv:1504.00915](#)].
- [49] R. J. Hill and M. P. Solon, *WIMP-nucleon scattering with heavy WIMP effective theory*, [arXiv:1309.4092](#).
- [50] J. Hisano, K. Ishiwata, N. Nagata, and T. Takesako, *Direct Detection of Electroweak-Interacting Dark Matter*, *JHEP* **1107** (2011) 005, [[arXiv:1104.0228](#)].
- [51] V. Barger, W.-Y. Keung, and D. Marfatia, *Electromagnetic properties of dark matter: Dipole moments and charge form factor*, *Phys. Lett.* **B696** (2011) 74–78, [[arXiv:1007.4345](#)].
- [52] T. Banks, J.-F. Fortin, and S. Thomas, *Direct Detection of Dark Matter Electromagnetic Dipole Moments*, [arXiv:1007.5515](#).
- [53] J.-F. Fortin and T. M. P. Tait, *Collider Constraints on Dipole-Interacting Dark Matter*, *Phys. Rev.* **D85** (2012) 063506, [[arXiv:1103.3289](#)].
- [54] A. Djouadi, *The Anatomy of electro-weak symmetry breaking. I: The Higgs boson in the standard model*, *Phys.Rept.* **457** (2008) 1–216, [[hep-ph/0503172](#)].
- [55] **ATLAS, CMS** Collaboration, G. Aad et al., *Combined Measurement of the Higgs Boson Mass in pp Collisions at $\sqrt{s} = 7$ and 8 TeV with the ATLAS and CMS Experiments*, *Phys. Rev. Lett.* **114** (2015) 191803, [[arXiv:1503.07589](#)].
- [56] M. E. Peskin and T. Takeuchi, *Estimation of oblique electroweak corrections*, *Phys.Rev.* **D46** (1992) 381–409.
- [57] R. Barbieri, A. Pomarol, R. Rattazzi, and A. Strumia, *Electroweak symmetry breaking after LEP-1 and LEP-2*, *Nucl. Phys.* **B703** (2004) 127–146, [[hep-ph/0405040](#)].
- [58] H. Mebane, N. Greiner, C. Zhang, and S. Willenbrock, *Constraints on Electroweak Effective Operators at One Loop*, *Phys. Rev.* **D88** (2013), no. 1 015028, [[arXiv:1306.3380](#)].
- [59] **Fermi-LAT** Collaboration, M. Ackermann et al., *Search for gamma-ray spectral lines with the Fermi large area telescope and dark matter implications*, *Phys. Rev.* **D88** (2013) 082002, [[arXiv:1305.5597](#)].
- [60] **Fermi-LAT** Collaboration, M. Ackermann et al., *Updated search for spectral lines from Galactic dark matter interactions with pass 8 data from the Fermi Large Area Telescope*, *Phys. Rev.* **D91** (2015), no. 12 122002, [[arXiv:1506.00013](#)].

- [61] **Fermi-LAT** Collaboration, M. Ackermann et al., *Searching for Dark Matter Annihilation from Milky Way Dwarf Spheroidal Galaxies with Six Years of Fermi-LAT Data*, *Phys. Rev. Lett.* **115** (2015), no. 23 231301, [[arXiv:1503.02641](#)].
- [62] **IceCube** Collaboration, M. G. Aartsen et al., *Improved limits on dark matter annihilation in the Sun with the 79-string IceCube detector and implications for supersymmetry*, *JCAP* **1604** (2016), no. 04 022, [[arXiv:1601.00653](#)].
- [63] **IceCube** Collaboration, M. G. Aartsen et al., *Search for dark matter annihilations in the Sun with the 79-string IceCube detector*, *Phys. Rev. Lett.* **110** (2013), no. 13 131302, [[arXiv:1212.4097](#)].
- [64] B. W. Lee and S. Weinberg, *Cosmological Lower Bound on Heavy Neutrino Masses*, *Phys. Rev. Lett.* **39** (1977) 165–168.
- [65] P. Hut, *Limits on Masses and Number of Neutral Weakly Interacting Particles*, *Phys. Lett.* **B69** (1977) 85.
- [66] D. Hooper, *Particle Dark Matter*, in *Proceedings of Theoretical Advanced Study Institute in Elementary Particle Physics on The dawn of the LHC era (TASI 2008)*, pp. 709–764, 2010. [arXiv:0901.4090](#).
- [67] G. Jungman, M. Kamionkowski, and K. Griest, *Supersymmetric dark matter*, *Phys.Rept.* **267** (1996) 195–373, [[hep-ph/9506380](#)].
- [68] E. W. Kolb and M. S. Turner, *The Early Universe*, *Front. Phys.* **69** (1990) 1–547.
- [69] S. Dodelson, *Modern Cosmology*. Academic Press, Amsterdam, 2003.
- [70] S. Weinberg, *Cosmology*. Oxford Univ. Press (2008), 2008.
- [71] J. Edsjo and P. Gondolo, *Neutralino relic density including coannihilations*, *Phys. Rev.* **D56** (1997) 1879–1894, [[hep-ph/9704361](#)].
- [72] K. Griest and D. Seckel, *Three exceptions in the calculation of relic abundances*, *Phys. Rev.* **D43** (1991) 3191–3203.
- [73] G. Belanger, F. Boudjema, and A. Pukhov, *micrOMEGAs : a code for the calculation of Dark Matter properties in generic models of particle interaction*, in *The Dark Secrets of the Terascale*, pp. 739–790, 2013. [arXiv:1402.0787](#).
- [74] A. Semenov, *LanHEP: A package for automatic generation of Feynman rules from the Lagrangian*, *Comput. Phys. Commun.* **115** (1998) 124–139.
- [75] D. Hooper, C. Kelso, and F. S. Queiroz, *Stringent and Robust Constraints on the Dark Matter Annihilation Cross Section From the Region of the Galactic Center*, *Astropart. Phys.* **46** (2013) 55–70, [[arXiv:1209.3015](#)].
- [76] J. F. Navarro, C. S. Frenk, and S. D. M. White, *The Structure of cold dark matter halos*, *Astrophys. J.* **462** (1996) 563–575, [[astro-ph/9508025](#)].
- [77] A. Sommerfeld, *Über die beugung und bremsung der elektronen*, *Annalen der Physik* **403** no. 3.

- [78] J. Hisano, S. Matsumoto, and M. M. Nojiri, *Explosive dark matter annihilation*, *Phys. Rev. Lett.* **92** (2004) 031303, [[hep-ph/0307216](#)].
- [79] J. Hisano, S. Matsumoto, M. M. Nojiri, and O. Saito, *Non-perturbative effect on dark matter annihilation and gamma ray signature from galactic center*, *Phys. Rev.* **D71** (2005) 063528, [[hep-ph/0412403](#)].
- [80] M. Cirelli, A. Strumia, and M. Tamburini, *Cosmology and Astrophysics of Minimal Dark Matter*, *Nucl. Phys.* **B787** (2007) 152–175, [[arXiv:0706.4071](#)].
- [81] **LUX** Collaboration, D. S. Akerib et al., *Results on the Spin-Dependent Scattering of Weakly Interacting Massive Particles on Nucleons from the Run 3 Data of the LUX Experiment*, *Phys. Rev. Lett.* **116** (2016), no. 16 161302, [[arXiv:1602.03489](#)].
- [82] **ATLAS** Collaboration, G. Aad et al., *Search for dark matter in events with a Z boson and missing transverse momentum in pp collisions at $\sqrt{s}=8$ TeV with the ATLAS detector*, *Phys. Rev.* **D90** (2014), no. 1 012004, [[arXiv:1404.0051](#)].
- [83] **ATLAS** Collaboration, G. Aad et al., *Search for new particles in events with one lepton and missing transverse momentum in pp collisions at $\sqrt{s} = 8$ TeV with the ATLAS detector*, *JHEP* **09** (2014) 037, [[arXiv:1407.7494](#)].
- [84] **CMS** Collaboration, V. Khachatryan et al., *Search for physics beyond the standard model in final states with a lepton and missing transverse energy in proton-proton collisions at $\sqrt{s} = 8$ TeV*, *Phys. Rev.* **D91** (2015), no. 9 092005, [[arXiv:1408.2745](#)].
- [85] **ATLAS** Collaboration, G. Aad et al., *Search for dark matter in events with a hadronically decaying W or Z boson and missing transverse momentum in pp collisions at $\sqrt{s} = 8$ TeV with the ATLAS detector*, *Phys. Rev. Lett.* **112** (2014), no. 4 041802, [[arXiv:1309.4017](#)].
- [86] A. G. Delannoy et al., *Probing Dark Matter at the LHC using Vector Boson Fusion Processes*, *Phys. Rev. Lett.* **111** (2013) 061801, [[arXiv:1304.7779](#)].
- [87] A. Berlin, T. Lin, M. Low, and L.-T. Wang, *Neutralinos in Vector Boson Fusion at High Energy Colliders*, *Phys. Rev.* **D91** (2015), no. 11 115002, [[arXiv:1502.05044](#)].
- [88] **ATLAS** Collaboration, G. Aad et al., *Search for invisible decays of a Higgs boson using vector-boson fusion in pp collisions at $\sqrt{s} = 8$ TeV with the ATLAS detector*, *JHEP* **01** (2016) 172, [[arXiv:1508.07869](#)].
- [89] **CMS** Collaboration, S. Chatrchyan et al., *Search for invisible decays of Higgs bosons in the vector boson fusion and associated ZH production modes*, *Eur. Phys. J.* **C74** (2014) 2980, [[arXiv:1404.1344](#)].
- [90] **CMS** Collaboration, V. Khachatryan et al., *Search for dark matter, extra dimensions, and unparticles in monojet events in proton–proton collisions at $\sqrt{s} = 8$ TeV*, *Eur. Phys. J.* **C75** (2015), no. 5 235, [[arXiv:1408.3583](#)].

- [91] **ATLAS** Collaboration, G. Aad et al., *Search for new phenomena in events with a photon and missing transverse momentum in pp collisions at $\sqrt{s} = 8$ TeV with the ATLAS detector*, *Phys. Rev.* **D91** (2015), no. 1 012008, [[arXiv:1411.1559](#)]. [Erratum: *Phys. Rev.*D92,no.5,059903(2015)].
- [92] J. Brooke, M. R. Buckley, P. Dunne, B. Penning, J. Tamanas, and M. Zgubic, *Vector Boson Fusion Searches for Dark Matter at the LHC*, [arXiv:1603.07739](#).
- [93] A. Belyaev, N. D. Christensen, and A. Pukhov, *CalcHEP 3.4 for collider physics within and beyond the Standard Model*, *Comput. Phys. Commun.* **184** (2013) 1729–1769, [[arXiv:1207.6082](#)].
- [94] A. Ismail, E. Izaguirre, and B. Shuve, *Illuminating New Electroweak States at Hadron Colliders*, *Phys. Rev.* **D94** (2016), no. 1 015001, [[arXiv:1605.00658](#)].
- [95] G. Busoni, A. De Simone, E. Morgante, and A. Riotto, *On the Validity of the Effective Field Theory for Dark Matter Searches at the LHC*, *Phys. Lett.* **B728** (2014) 412–421, [[arXiv:1307.2253](#)].
- [96] G. Busoni, A. De Simone, J. Gramling, E. Morgante, and A. Riotto, *On the Validity of the Effective Field Theory for Dark Matter Searches at the LHC, Part II: Complete Analysis for the s-channel*, *JCAP* **1406** (2014) 060, [[arXiv:1402.1275](#)].
- [97] O. Buchmueller, M. J. Dolan, and C. McCabe, *Beyond Effective Field Theory for Dark Matter Searches at the LHC*, *JHEP* **01** (2014) 025, [[arXiv:1308.6799](#)].
- [98] M. Endo and Y. Yamamoto, *Unitarity Bounds on Dark Matter Effective Interactions at LHC*, *JHEP* **06** (2014) 126, [[arXiv:1403.6610](#)].
- [99] N. Bell, G. Busoni, A. Kobakhidze, D. M. Long, and M. A. Schmidt, *Unitarisation of EFT Amplitudes for Dark Matter Searches at the LHC*, [arXiv:1606.02722](#).
- [100] M. Duch, B. Grzadkowski, and J. Wudka, *Classification of effective operators for interactions between the Standard Model and dark matter*, *JHEP* **05** (2015) 116, [[arXiv:1412.0520](#)].
- [101] B. Grzadkowski, M. Iskrzynski, M. Misiak, and J. Rosiek, *Dimension-Six Terms in the Standard Model Lagrangian*, *JHEP* **10** (2010) 085, [[arXiv:1008.4884](#)].
- [102] W.-C. Huang and F. F. Deppisch, *Dark matter origins of neutrino masses*, *Phys. Rev.* **D91** (2015) 093011, [[arXiv:1412.2027](#)].